Regular Article - Theoretical Physics

Gravitational lensing by a black-bounce-Reissner–Nordström spacetime

Jing Zhang[1], **Yi Xie**[2,a]

[1] School of Astronomy and Space Science, Nanjing University, Nanjing 210023, China
[2] Purple Mountain Observatory, Chinese Academy of Sciences, Nanjing 210023, China

Abstract We investigate the weak and strong deflection gravitational lensing by a black-bounce-Reissner–Nordström spacetime and obtain their lensing observables. Assuming the supermassive black holes in the Galactic Center and at the center of M87, Sgr A* and M87* respectively, as the lenses, we evaluate these observables and assess their detectability. We also intensively compare these lensing signatures with those of various tidal or charged spacetimes. We find that it might be possible to distinguish these spacetimes by measuring the fluxes difference of the lensed images by Sgr A* in its quiet stage.

1 Introduction

Black holes are demonstrated to be very common in the Universe by detection of their gravitational waves [1–6] and by the direct image of the supermassive black hole M87* in the center of galaxy M87 [7–12]. They are also thought as ideal places for examining and testing current understanding of gravitation in the strong field. Though a black hole is considered as the simplest celestial body in Einstein's general relativity, it is harmed by its event horizon and central singularity, which would trigger the information-loss problem and break the general relativity down. A number of proposals have been suggested to get rid of the singularity, such as building a regular core [13–16], bouncing by quantum pressure [17–19] and forming a quasi-black hole [20–23] (see Ref. [24] for a review).

In the past few years, a black-bounce-Schwarzschild spacetime was introduced [25]. It can smoothly transition from a regular black hole (a black bounce) to a traversable wormhole. In the massless case, it reduces to the Ellis wormhole [26]. Such an idea has attracted much attention. It was extended to a time-dependent case [27], to a spherically sym-

metric thin-shell traversable wormhole [28] and to several new classes [29]. Its quasinormal modes [30], absorption of massless scalar waves [31], geodesic motion [32], thin accretion disk [33] and gravitational lensing [34–37] were studied. Recently, a charged black-bounce variant of the Reissner–Nordström spacetime was constructed [38]. Such a black-bounce-Reissner–Nordström spacetime is considered as a simple and clean everywhere-regular black hole mimicker, whose deviation from the Reissner–Nordström spacetime is in a precisely controlled and minimal manner, and it can be interpreted as standard Maxwell electromagnetism together with an anisotropic fluid [38]. It is widely believed that an astrophysical body in the real Universe has to be free of electric charges due to quick neutralization by the surrounding plasma. However, a black hole might be charged by inheriting from its charged collapsed progenitor [39], by accumulating charged matter and by induction through its rotation in the external magnetic field [40]. It was pointed [41] that the supermassive black hole in the Galactic center, Sgr A*, might have transient and small positive charge. Therefore, besides a significant theoretical impact, the non-zero electric charge might make the black-bounce-Reissner–Nordström spacetime show distinctive observable characters. In this work, we will comprehensively investigate the gravitational-lensing signatures of the black-bounce-Reissner–Nordström spacetime, which is still barely known in the literature except few brief discussion about its photon rings [42] and deflection angle in the weak field limit [43].

Gravitational lensing bends the trajectory of a photon passing through gravitational field and delays the arrival time of the photon, so that it is considered as a powerful probe for examining the spacetime of a distant object [44]. According to the deflection angle, the gravitational lensing might roughly be divided into two scenarios. As particularly useful tools in astronomy [45–48] and in gravitational physics [49–52], the weak deflection gravitational lensing has its deflection angle much less than unity. Allowing photons to wind

ᵃ e-mail: yixie@pmo.ac.cn (corresponding author)

around a compact object by a few times and forming relativistic images in its vicinity [53], the strong deflection gravitational lensing has its deflection angle much bigger than 1. The direct image of M87* by the Event Horizon Telescope (EHT) [7–12] shows the feasibility of measuring effects of the strong deflection gravitational lensing by black holes and its potential for understanding the black hole physics [54–61], testing various kinds of black holes [62–65] and probing horizonless compact objects [66–83].

Triggered by previous works [84–91], we will investigate the weak and strong deflection gravitational lensing by the black-bounce-Reissner–Nordström spacetime for a whole picture of its lensing signatures, which would be helpful for detecting and searching them. In the meantime, we will carefully compare its observables with those of various tidal/charged black holes, such as the Reissner–Nordström black hole [92,93], the tidal Reissner–Nordström black hole [94], the charged Horndeski black hole [95] and the charged Galileon black hole [96]. The gravitational lensing of these black holes have been well studied in Refs. [49,56,57,97,98], Refs. [99–103], Ref. [104] and Ref. [105], respectively. We will intensively discuss the possibility of distinguishing these spacetimes with the current successful technology of radio and infrared interferometry, such as EHT [7] and GRAVITY [106].

This paper is structured as follows. In Sect. 2, we briefly review the spacetime of the black-bounce-Reissner–Nordström spacetime and the essentials of the gravitational lensing. In Sects. 3 and 4, we investigate its weak and strong deflection gravitational lensing, respectively. We find its lensing observables and discuss their observability by assuming Sgr A* and M87* as lenses (if applicable). We also compare its lensing signatures with those of other tidal or charged spacetimes and evaluate the feasibility of distinguishing them. Conclusions and discussion are presented in Sect. 5.

2 Spacetime and gravitational lensing

2.1 Spacetime

As a black-bounce variant of a charged black hole, a black-bounce-Reissner–Nordström spacetime can be constructed with the Reissner–Nordström spacetime, which is taken as the solution to the electrovac Einstein field equations of general relativity in standard (t, r, θ, φ) curvature coordinates, by the following steps [38]. First, leave $\mathrm{d}r$ in the metric tensor unchanged; and second, replace r with $\sqrt{r^2 + l_\bullet^2}$ in which the components of the metric have an explicit dependence of r. Here, $l_\bullet$ is a length scale, also called the bounce parameter, which is related to the Planck length. Therefore, the metric of the black-bounce-Reissner–Nordström spacetime with the

mass $m_\bullet$ and the charge $Q_\bullet$ was found as [38]

$$\mathrm{d}s^2 = -A(r)\mathrm{d}t^2 + B(r)\mathrm{d}r^2 + C(r)(\mathrm{d}\theta^2 + \sin^2\theta\,\mathrm{d}\varphi^2), \quad (1)$$

where

$$A(r) = [B(r)]^{-1} = 1 - \frac{2m_\bullet}{\sqrt{r^2 + l_\bullet^2}} + \frac{Q_\bullet^2}{r^2 + l_\bullet^2}, \quad (2)$$

$$C(r) = r^2 + l_\bullet^2. \quad (3)$$

This spacetime can be interpreted as standard Maxwell electromagnetism with an anisotropic fluid and the general relativity is reasonably assumed to be valid at least sufficiently far away from its core region [38]. It is asymptotically flat as $|r| \to \pm\infty$ and globally regular due to the existence of the bounce parameter $l_\bullet$ that smooths the original Reissner–Nordström spacetime. Such a bounce parameter also characterizes the interpolation between the Reissner–Nordström spacetime and the traversable wormhole. When $l_\bullet = 0$, the black-bounce-Reissner–Nordström spacetime returns to the Reissner–Nordström spacetime. As the charge vanishes, i.e., $Q_\bullet = 0$, one arrives at the black-bounce-Schwarzschild spacetime [25]. When $m_\bullet = 0$ and $Q_\bullet = 0$, the spacetime (1) goes back to the Ellis wormhole [26]. As $Q_\bullet = 0$ and $l_\bullet = 0$, one recovers the Schwarzschild black hole.

The outer and inner event horizons for the spacetime (1) are respectively located at [38]

$$r_\pm = \sqrt{\left(m_\bullet \pm \sqrt{m_\bullet^2 - Q_\bullet^2}\right)^2 - l_\bullet^2}, \quad (4)$$

which requires

$$Q_\bullet^2 \le m_\bullet^2 \quad \text{and} \quad l_\bullet^2 \le \left(m_\bullet \pm \sqrt{m_\bullet^2 - Q_\bullet^2}\right)^2 \quad (5)$$

for the existence of positive $r_\pm$. In order to investigate the possibility of distinguishing the black-bounce-Reissner–Nordström spacetime from other tidal or charged black holes, such as the Reissner–Nordström black hole, the tidal Reissner–Nordström black hole, the charged Galileon black hole and the charged Horndeski black hole, we will focus on a subclass of the black-bounce-Reissner–Nordström spacetime that has its event horizon(s) in this work. The gravitational lensing by a horizonless black-bounce-Reissner–Nordström spacetime will be left as our next move. For later convenience, we define the following dimensionless quantities as

$$x = \frac{r}{m_\bullet}, \quad l = \frac{l_\bullet^2}{m_\bullet^2} \quad \text{and} \quad q = \frac{Q_\bullet^2}{m_\bullet^2}, \quad (6)$$

and the rescaled bounce parameter as

$$\lambda = \frac{l}{(1 + \sqrt{1 - q})^2}, \quad (7)$$

so that the condition for the outer event horizon (5) can be rewritten as

$$\mathcal{D}_H = \{(q, \lambda) \mid 0 \leq q \leq 1, \ 0 \leq \lambda \leq 1\} \tag{8}$$

and the dimensionless radius of the outer event horizon can be defined as

$$x_H = \frac{r_+}{m_\bullet} = \sqrt{1 - \lambda}(1 + \sqrt{1 - q}). \tag{9}$$

The left panel of Fig. 1 shows that x_H decreases with the growth of q and λ. When both the charge and the bounce parameter disappear, i.e., $q = \lambda = 0$, the spacetime (1) will have its biggest event horizon, i.e., $x_H = 2$, which is the same as the one of the Schwarzschild black hole. Otherwise, the outer event horizon shrinks until it vanishes as $\lambda = 1$. The right panel of Fig. 1 demonstrates a comparison of x_H against q for the black-bounce-Reissner–Nordström spacetime, the Reissner–Nordström black hole, the tidal Reissner–Nordström black hole, the charged Horndeski black hole and the charged Galileon black hole, among which the Reissner–Nordström black hole and the charged Galileon black hole share the same x_H. With the increment of q, x_H becomes smaller for all of these spacetimes. For a given q, the black-bounce-Reissner–Nordström spacetime has the smallest event horizon x_H, while a smaller λ, i.e., a smaller rescaled bounce parameter, can make x_H of the black-bounce-Reissner–Nordström spacetime more significantly deviate from those of other black holes. The tidal Reissner–Nordström black hole is able to have the biggest event horizon since its tidal charge q can be negative.

The photon sphere of the black-bounce-Reissner–Nordström spacetime sets the innermost circular orbit for a photon and casts the shadow that might be able to observe by EHT. With the direct image of M87* [7–12], the angular size of its photon sphere was found to be consistent within 17% with the prediction by the general relativity [107]. Following this approach, we might test the black-bounce-Reissner–Nordström spacetime and other spacetimes in their strong-field regime and obtain preliminary bounds on their (dimensionless) charge. Although the metrics for the black-bounce-Reissner–Nordström spacetime, the Reissner–

Nordström black hole, the charged Horndeski black hole and the charged Galileon black hole have very different dependence of q, the radii of their photon spheres surprisedly share almost the same numerical value for a specific q so that we find the bound on q for these spacetimes as (see Sect. 4.1 for details)

$$\mathcal{D} = \{q \mid 0 \leq q \leq 0.8144\}. \tag{10}$$

Furthermore, we find the bound for the tidal Reissner–Nordström black hole as

$$\mathcal{D}_{TRN} = \{q \mid -1.2198 \leq q \leq 0.8144\}. \tag{11}$$

These two bounds will be taken in the following investigation on the weak and strong deflection gravitational lensing by these spacetimes and for comparing their observability.

2.2 Gravitational lensing

In the black-bounce-Reissner–Nordström spacetime (1), the light deflection angle $\hat{\alpha}$ can be obtained as [54,108]

$$\hat{\alpha}(r_0) = 2 \int_{r_0}^{\infty} \frac{dr}{\sqrt{C(r)[C(r)u^{-2} - A(r)]}} - \pi, \tag{12}$$

where r_0 is the closest approach of the light, u is the impact parameter as

$$u^2 = \frac{C(r_0)}{A(r_0)}, \tag{13}$$

and $A(r)B(r) = 1$ has been applied. When r_0 is much bigger than $m_\bullet$, we can have $\hat{\alpha} \ll 1$ for the weak deflection gravitational lensing. When r_0 is comparable to $m_\bullet$, we can find $\hat{\alpha} \gg 1$ for the strong deflection gravitational lensing.

For description about the geometric relation among the source, the lensed images, the lens and the observer, we take the following lensing equation as [54,55]

$$\tan \mathcal{B} = \tan \vartheta - \frac{D_{LS}}{D_{OS}}[\tan \vartheta + \tan(\hat{\alpha} - \vartheta)], \tag{14}$$

where D_{OS} and D_{LS} are the distances from the source to the observer and to the lens, respectively, and ϑ and $\mathcal{B}$ are the angular positions of the lensed images and the source,

Fig. 1 Left panel: The dimensionless radius x_H of the outer event horizon for the black-bounce-Reissner–Nordström spacetime with respect to q and λ. Right panel: A comparison of x_H among the black-bounce-Reissner–Nordström spacetime (bbRN), the Reissner–Nordström black hole (RN), the tidal Reissner–Nordström black hole (TRN), the charged Horndeski black hole (CH) and the charged Galileon black hole (CG)
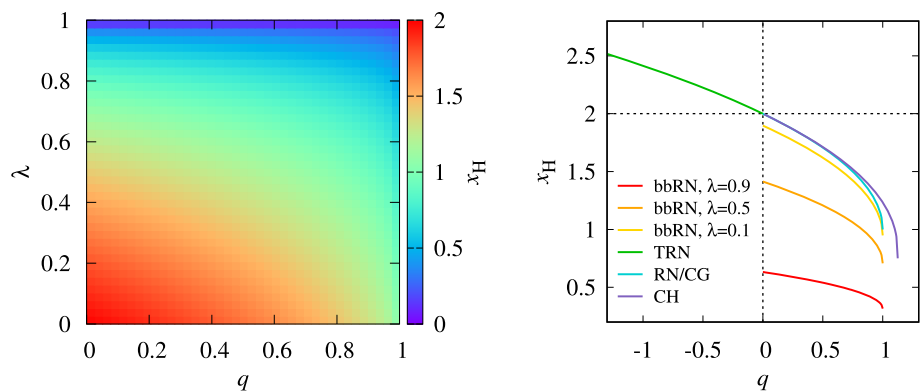
respectively. The magnification of the image μ is defined as [109]

$$\mu(\vartheta) = \left[\frac{\sin\mathcal{B}(\vartheta)}{\sin\vartheta} \frac{d\mathcal{B}(\vartheta)}{d\vartheta} \right]^{-1}, \tag{15}$$

which indicates the flux ratio of the lensed image to the unlensed one.

If the brightness of the source would change with time, another observable is the time delay between the two lensed images, which relies on the flight time of the photon traveling from the source to the observer [108]

$$T = T(R_{src}) + T(R_{obs}), \tag{16}$$

where R_{src} is the radial distance from the source to the lens as

$$R_{src} = \sqrt{D_{LS}^2 + D_{OS}^2 \tan^2 \mathcal{B}}, \tag{17}$$

and $R_{obs} = D_{OL}$ is the distance from the observer to the lens. The function of $T(R)$ reads [54,108]

$$T(R) = \int_{r_0}^{R} \frac{\sqrt{C(r)} dr}{A(r)\sqrt{C(r) - u^2 A(r)}}, \tag{18}$$

where the relation $A(r)B(r) = 1$ has also been used.

In the following sections, we will intensively investigate the weak and strong deflection gravitational lensing by the black-bounce-Reissner–Nordström spacetime. Since ground-based telescopes have been routinely observing stars around Sgr A* in the optical/near-infrared band and EHT has directly imaged M87* in the radio band, these two supermassive black holes will be taken as the lenses (if applicable) for evaluation of the lensing observables. We will also carefully compare these observables with those of other tidal or charged black holes and comprehensively discuss the possibility of distinguishing these spacetimes.

3 Weak deflection gravitational lensing

For the scenario of the weak deflection gravitational lensing, the closest approach of the light ray r_0 is much larger than the gravitational radius of the lens $m_\bullet$ so that we treat $m_\bullet r_0^{-1} \ll 1$ as a small parameter for our investigation in this section.

3.1 Deflection angle

With the standard procedure [108], we can find the deflection angle $\hat{\alpha}$ (19) as

$$\hat{\alpha}(r_0) = 4\frac{m_\bullet}{r_0} + \left(\frac{15}{4}\pi - \frac{3}{4}\pi q + \frac{1}{4}\pi l - 4 \right) \frac{m_\bullet^2}{r_0^2}$$
$$+ \left[\frac{122}{3} - \frac{15}{2}\pi + \left(\frac{3}{2}\pi - 14 \right) q \right.$$
$$\left. - \left(\frac{1}{2}\pi - \frac{2}{3} \right) l \right] \frac{m_\bullet^3}{r_0^3} + \mathcal{O}\left(\frac{m_\bullet^4}{r_0^4} \right). \tag{19}$$

The charge has its effect on the deflection angle starting from the term of $m_\bullet^2 r_0^{-2}$, and this situation also happens in the cases of the Reissner–Nordström black hole, the tidal Reissner–Nordström black hole, the charged Horndeski black hole and the charged Galileon black hole.

Since r_0 is coordinate-dependent, we can replace it with the impact parameter u that is gauge-invariant. After expanding Eq. (13) in terms of the small parameter $m_\bullet u^{-1}$ and rearranging it, we can have that

$$\frac{r_0}{u} = 1 - \frac{m_\bullet}{u} - \left(\frac{3}{2} - \frac{q}{2} + \frac{l}{2} \right) \frac{m_\bullet^2}{u^2}$$
$$- \left(4 - 2q + \frac{l}{2} \right) \frac{m_\bullet^3}{u^3} - \left(\frac{105}{8} + \frac{5}{8}q^2 \right.$$
$$\left. + \frac{1}{8}l^2 - \frac{1}{4}ql - \frac{35}{4}q + \frac{5}{4}l \right) \frac{m_\bullet^4}{u^4} + \mathcal{O}\left(\frac{m_\bullet^5}{u^5} \right). \tag{20}$$

Substituting it into the deflection angle $\hat{\alpha}(r_0)$, we find that

$$\hat{\alpha}(u) = 4\frac{m_\bullet}{u} + \left(\frac{15}{4}\pi - \frac{3}{4}\pi q + \frac{1}{4}\pi l \right) \frac{m_\bullet^2}{u^2}$$
$$+ \left(\frac{128}{3} - 16q + \frac{8}{3}l \right) \frac{m_\bullet^3}{u^3} + \mathcal{O}\left(\frac{m_\bullet^4}{u^4} \right). \tag{21}$$

It is clear that the charge and the bounce parameter also start to influence the deflection angle $\hat{\alpha}(u)$ from the term of $m_\bullet^2 u^{-2}$.

3.2 Positions of lensed images

For later convenience, we define the dimensionless variables [49]

$$\beta = \frac{\mathcal{B}}{\vartheta_E}, \quad \theta = \frac{\vartheta}{\vartheta_E}, \quad \varepsilon = \frac{\vartheta_\bullet}{\vartheta_E}, \tag{22}$$

where ϑ_E denotes the angular Einstein ring radius

$$\vartheta_E = \sqrt{\frac{4m_\bullet D_{LS}}{D_{OL} D_{OS}}}. \tag{23}$$

Therefore, β and θ are the dimensionless angular positions of the source and of the image seen by the observer, respectively. The opening angle of the gravitational radius $m_\bullet$ at the observer from the distance D_{OL} is defined as $\vartheta_\bullet = \arctan(m_\bullet D_{OL}^{-1})$. Since it is assumed that both the observer and the source are far away from the lens, the ratio

ε is a small parameter in the weak deflection gravitational lensing.

The position of the lensed image θ can be expanded in terms of ε as [49]

$$\theta = \theta_0 + \varepsilon\theta_1 + \varepsilon^2\theta_2 + \mathcal{O}\left(\varepsilon^3\right). \tag{24}$$

Substituting it into the lens equation (14) and using the deflection angle $\hat{\alpha}(u)$ (21), we can obtain the coefficients θ_n ($n = 0, 1, 2$) at the order of ε^n for the black-bounce-Reissner–Nordström spacetime as

$$\theta_0 = \frac{1}{2}\left(\beta + \eta\right), \tag{25}$$

$$\theta_1 = \frac{15 - 3q + l}{16\left(\theta_0^2 + 1\right)}\pi, \tag{26}$$

$$\theta_2 = \frac{1}{\theta_0\left(\theta_0^2 + 1\right)^3}\left[\frac{8}{3}D^2\theta_0^8 + \left(\frac{64}{3}D - 16\right)D\theta_0^6\right.$$
$$+ \left(\frac{88}{3}D^2 - 32D + 16\right)\theta_0^4 + \left(\frac{16}{3}D^2 - 16D\right.$$
$$\left. - \frac{225}{128}\pi^2 + 32\right)\theta_0^2 - \frac{16}{3}D^2 - \frac{225}{256}\pi^2 + 16$$
$$- \frac{\pi^2}{128}\left(\frac{1}{2} + \theta_0^2\right)(l - 3q)(l - 3q + 30)$$
$$\left. + 2\left(\theta_0^2 + 1\right)^2\left(\frac{l}{3} - 2q\right)\right], \tag{27}$$

where

$$D = \frac{D_{\mathrm{LS}}}{D_{\mathrm{OS}}}, \tag{28}$$

and

$$\eta = \sqrt{\beta^2 + 4}. \tag{29}$$

We can see that θ_0 remains unchanged as the one of the Schwarzschild black hole [49]. Although the charge and the bounce parameter cannot affect θ_0, they show their combined effect on the first-order term θ_1. If this next-to-leading-order term in the position of the lensed image might be detected, it would be possible to distinguish the black-bounce-Reissner–Nordström spacetime from the Schwarzschild black hole. However, any attempt to separate the contributions from the charge q and the bounce parameter l must have the ability to access the second order term θ_2, requiring exceedingly challenging accuracy for astrometry.

Following the convention adopted in Ref. [49], we set the angular positions of the lensed images to be positive. The lensed image is positive-parity, indicated by "+", if it is on the same side of the source with respect to the lens and the position angle of the source is positive, i.e., $\beta > 0$. Otherwise, the lensed image is negative-parity, indicated by "−", with $\beta < 0$.

The positions of the positive- and negative-parity images $\theta_n^{\pm}$ can, therefore, be found as

$$\theta_0^{\pm} = \frac{1}{2}\left(\eta \pm |\beta|\right), \tag{30}$$

$$\theta_1^{\pm} = \frac{15 - 3q + l}{8\eta\left(\eta \pm |\beta|\right)}\pi, \tag{31}$$

$$\theta_2^{\pm} = \frac{1}{\eta^3\left(\eta \pm |\beta|\right)^4}\left[\frac{64}{3}D^2\beta^8 + \left(\frac{1024}{3}D - 128\right)D\beta^6\right.$$
$$+ \left(\frac{5056}{3}D^2 - 1024D + 128\right)\beta^4$$
$$+ \left(\frac{8576}{3}D^2 - 2304D - \frac{225}{16}\pi^2 + 768\right)\beta^2$$
$$+ \frac{2560}{3}D^2 - 1024D - \frac{675}{16}\pi^2 + 1024$$
$$- \frac{\pi^2}{16}\left(\beta^2 + 3\right)(l - 3q)(l - 3q + 30)$$
$$\left. + 16\left(\beta^2 + 2\right)\left(\beta^2 + 4\right)\left(\frac{l}{3} - 2q\right)\right]$$
$$\pm \frac{\eta|\beta|}{\eta^3\left(\eta \pm |\beta|\right)^4}\left[\frac{64}{3}D^2\beta^6 + \left(\frac{896}{3}D - 128\right)D\beta^4\right.$$
$$+ \left(\frac{3392}{3}D^2 - 768D + 128\right)\beta^2$$
$$+ \frac{3328}{3}D^2 - 1024D - \frac{225}{16}\pi^2 + 512$$
$$- \frac{\pi^2}{16}(l - 3q)(l - 3q + 30)$$
$$\left. - 16\left(\beta^2 + 4\right)\left(\frac{l}{3} - 2q\right)\right], \tag{32}$$

which lead to the following relations

$$\theta_0^+\theta_0^- = 1, \tag{33}$$

$$\theta_0^+ - \theta_0^- = |\beta|, \tag{34}$$

$$\theta_1^+ + \theta_1^- = \frac{15 - 3q + l}{16}\pi, \tag{35}$$

$$\theta_1^+ - \theta_1^- = -\frac{(15 - 3q + l)|\beta|}{16\eta}\pi, \tag{36}$$

$$\theta_2^+ - \theta_2^- = |\beta|\left[8D^2 - 16 + \frac{225}{256}\pi^2\right.$$
$$\left. + \frac{\pi^2}{256}(l - 3q)(l - 3q + 30) - \frac{2}{3}l + 4q\right]. \tag{37}$$

The zero-order term $\theta_0^{\pm}$ and the relations between them are not influenced by the charge and the bounce parameter, while the first- and second-order terms $\theta_1^{\pm}$ and $\theta_2^{\pm}$ and their relations $\theta_1^+ + \theta_1^-$ and $\theta_1^+ - \theta_1^-$ are all affected.

3.3 Magnification

The magnification μ (15) might be expanded in terms of ε as [49]

$$\mu = \mu_0 + \varepsilon\mu_1 + \varepsilon^2\mu_2 + \mathcal{O}(\varepsilon^3). \tag{38}$$

By making use of θ (24), one can obtain the coefficients μ_i as

$$\mu_0 = \frac{\theta_0^4}{\theta_0^4 - 1}, \tag{39}$$

$$\mu_1 = -\frac{(15 - 3q + l)\,\pi}{16\left(\theta_0^2 + 1\right)^3}\theta_0^3, \tag{40}$$

$$\mu_2 = \frac{\theta_0^2}{\left(\theta_0^2 + 1\right)^5\left(\theta_0^2 - 1\right)}\left[\frac{8}{3}D^2\theta_0^8\right.$$
$$+\left(48D^2 - 32D - 32\right)\theta_0^6$$
$$+\left(\frac{272}{3}D^2 - 64D + \frac{675}{128}\pi^2 - 64\right)\theta_0^4$$
$$+\left(48D^2 - 32D - 32\right)\theta_0^2 + \frac{8}{3}D^2$$
$$+\frac{3}{128}\pi^2\theta_0^4\,(l - 3q)\,(l - 3q + 30)$$
$$\left.-4\left(1 + \theta_0^2\right)^2\theta_0^2\left(\frac{l}{3} - 2q\right)\right]. \tag{41}$$

Likewise, the leading term of the magnification μ_0 is not changed by the charge and the bounce parameter, while the higher order terms μ_1 and μ_2 contain their contributions.

With the magnification (38), one can find $\mu_n^{\pm}$ for the positive- and negative-parity images as

$$\mu_0^{\pm} = \frac{1}{2} \pm \frac{\beta^2 + 2}{2|\beta|\eta}, \tag{42}$$

$$\mu_1^+ = \mu_1^- = -\frac{15 - 3q + l}{16\eta^3}\pi, \tag{43}$$

$$\mu_2^{\pm} = \pm\frac{1}{|\beta|\eta^5}\left[\frac{8}{3}D^2\beta^4 + \left(\frac{176}{3}D^2 - 32D - 32\right)\beta^2\right.$$
$$+192D^2 - 128D + \frac{675}{128}\pi^2 - 128$$
$$+\frac{3}{128}\pi^2\,(l - 3q)\,(l - 3q + 30)$$
$$\left.-4\left(\beta^2 + 4\right)\left(\frac{l}{3} - 2q\right)\right], \tag{44}$$

which have the relations

$$\mu_0^+ + \mu_0^- = 1, \tag{45}$$

$$\mu_0^+ - \mu_0^- = \frac{\beta^2 + 2}{|\beta|\eta}, \tag{46}$$

$$\mu_1^+ - \mu_1^- = 0, \tag{47}$$

$$\mu_2^+ + \mu_2^- = 0. \tag{48}$$

The charge and the bounce parameter appear in the first- and second-order terms $\mu_1^{\pm}$ and $\mu_2^{\pm}$ but do not affect the zero-order term $\mu_0^{\pm}$. However, the combinations mentioned above are immune to the charge and the bounce parameter.

3.4 Total magnification and centroid

In practice, the positive- and negative-parity images might be unable to resolve so that their total magnification and centroid would instead be the observables. The total magnification is defined as

$$\mu_{\text{tot}} = |\mu^+| + |\mu^-| = \mu^+ - \mu^-$$
$$= \frac{\beta^2 + 2}{|\beta|\eta} + 2\varepsilon^2\mu_2^+ + \mathcal{O}(\varepsilon^3). \tag{49}$$

Its leading term relies on the angular position of the source only, while the charge and the bounce parameter start to act from the second-order term μ_2^+. Owning to the relation (47), the first-order term in the total magnification will never exist. Therefore, it would be very challenging to distinguish these tidal/charged spacetimes by measuring the second-order term in the total magnification.

The centroid Θ_{cent} is the weighted average of the magnification by the positions of the two lensed images, which reads

$$\Theta_{\text{cent}} = \frac{\theta^+|\mu^+| - \theta^-|\mu^-|}{|\mu^+| + |\mu^-|} = \frac{\theta^+\mu^+ + \theta^-\mu^-}{\mu^+ - \mu^-}. \tag{50}$$

It can be expanded in terms of ε as

$$\Theta_{\text{cent}} = \frac{|\beta|(\beta^2 + 3)}{\beta^2 + 2} + \frac{|\beta|\varepsilon^2}{(\beta^2 + 2)^2\eta^2}\left[\frac{8}{3}D^2\beta^6\right.$$
$$+\left(\frac{104}{3}D^2 - 16D\right)\beta^4$$
$$+\left(\frac{272}{3}D^2 - 64D + 32\right)\beta^2$$
$$-\frac{64}{3}D^2 + 128 - \frac{675}{128}\pi^2$$
$$-\frac{3}{128}\pi^2\,(l - 3q)\,(l - 3q + 30)$$
$$\left.+4\left(\beta^2 + 4\right)\left(\frac{l}{3} - 2q\right)\right] + \mathcal{O}(\varepsilon^3). \tag{51}$$

Like the total magnification, the leading term of the centroid Θ_{cent} is not influenced, and its first-order term vanishes. The charge and the bounce parameter start to play their roles on the second-order term of the centroid.

3.5 Time delay

Due to $h = m_{\bullet}r_0^{-1} \ll 1$ in the weak deflection gravitational lensing, the time function $T(R)$ (18) can be expanded in

terms of h as

$$T(R) = T_0 + r_0 T_1 h + r_0 T_2 h^2 + r_0 T_3 h^3 + \mathcal{O}(h^4), \quad (52)$$

where

$$T_0 = \sqrt{R^2 - r_0^2}, \quad (53)$$

$$T_1 = \frac{\sqrt{1-\xi^2}}{1+\xi} + 2\log\left(\frac{1+\sqrt{1-\xi^2}}{\xi}\right), \quad (54)$$

$$T_2 = \frac{15}{2}\arccos\xi - \left(2 + \frac{5}{2}\xi\right)\frac{\sqrt{1-\xi^2}}{(1+\xi)^2}$$
$$+ \frac{l-3q}{2}\arccos\xi, \quad (55)$$

$$T_3 = -\frac{15}{2}\arccos\xi + \frac{1}{2}\frac{\sqrt{1-\xi^2}}{(1+\xi)^3}$$
$$\times \left(35\xi^3 + 133\xi^2 + 157\xi + 60\right)$$
$$+ \left(-\frac{1}{2}\arccos\xi + \frac{\sqrt{1-\xi^2}}{1+\xi}\right)(l-3q)$$
$$-\frac{1}{2}\sqrt{1-\xi^2}\frac{16+15\xi}{1+\xi}q, \quad (56)$$

with

$$\xi = \frac{r_0}{R}. \quad (57)$$

As those of the Schwarzschild black hole [49], the geometric term T_0 and the Shapiro delay term T_1 are not influenced by the charge q and the bounce parameter l, which affect the second- and third-order terms T_2 and T_3.

The difference between the flight time of a photon travelling from the source to the observer with and without the gravitational lensing is defined as the time delay [49]

$$c\tau = T(R_{\mathrm{src}}) + T(R_{\mathrm{obs}}) - \frac{D_{\mathrm{OS}}}{\cos\mathcal{B}}. \quad (58)$$

After rescaling by the characteristic time

$$\tau_{\mathrm{E}} = \frac{4m_\bullet}{c}, \quad (59)$$

the dimensionless time delay can also be expanded in terms of ε as

$$\hat{\tau} = \frac{\tau}{\tau_{\mathrm{E}}} = \hat{\tau}_0 + \varepsilon\hat{\tau}_1 + \varepsilon^2\hat{\tau}_2 + \mathcal{O}(\varepsilon^3), \quad (60)$$

where

$$\hat{\tau}_0 = \frac{1}{2}\left[1 + \beta^2 - \theta_0^2 - \ln\left(\frac{D_{\mathrm{OL}}\theta_0^2\vartheta_{\mathrm{E}}^2}{4D_{\mathrm{LS}}}\right)\right], \quad (61)$$

$$\hat{\tau}_1 = \frac{(15 + l - 3q)\pi}{16\theta_0}, \quad (62)$$

$$\hat{\tau}_2 = \frac{1}{\theta_0^2}\left\{\left(-\frac{10}{3}D^2 + 6D - 2\right)\theta_0^6 + 4(1-D)\beta^2\theta_0^4\right.$$
$$+ \left[\left(\frac{10}{3}D^2 - 2D - 2\right)\beta^4 + 4\beta^2 - 16D^2\right.$$

$$\left. + 16D - 4\right]\theta_0^2 + \frac{16}{3}D^2 - \frac{225\pi^2}{512(1+\theta_0^2)}$$
$$+ \frac{1}{3}(l - 3q) - \frac{(l-3q)(l-3q+30)\pi^2}{512(1+\theta_0^2)}$$
$$+ (\theta_0^2 - 1)q\bigg\}. \quad (63)$$

The charge and the bounce parameter begin to affect the time delay $\hat{\tau}$ from the first-order term of ε.

The time delay $\hat{\tau}$ is not an observable because the flight time of a photon without the gravitational lensing is unknown. However, the differential time delay $\Delta\hat{\tau}$ between the positive- and negative-parity images is practically measurable and it reads

$$\Delta\hat{\tau} = \hat{\tau}^+ - \hat{\tau}^- = \Delta\hat{\tau}_0 + \varepsilon\Delta\hat{\tau}_1 + \varepsilon^2\Delta\hat{\tau}_2 + \mathcal{O}(\varepsilon^3), \quad (64)$$

where

$$\Delta\hat{\tau}_0 = \frac{1}{2}\eta|\beta| + \ln\left(\frac{\eta + |\beta|}{\eta - |\beta|}\right), \quad (65)$$

$$\Delta\hat{\tau}_1 = \frac{15 + l - 3q}{16}\pi|\beta|, \quad (66)$$

$$\Delta\hat{\tau}_2 = |\beta|\eta\left\{\left(\frac{10}{3}D^2 - 2D - 2\right)\beta^2\right.$$
$$- \frac{225\pi^2}{512\eta^2}\left(\beta^2 + 3\right) + 12D^2 - 12D + 4$$
$$- \frac{\pi^2(\beta^2 + 3)}{512\eta^2}(l - 3q)(l - 3q + 30)$$
$$+ \frac{1}{3}l - 2q\bigg\}. \quad (67)$$

Its leading term $\Delta\hat{\tau}_0$ is the same as the one of the Schwarzschild black hole [49], while its first- and second-order terms $\Delta\hat{\tau}_1$ and $\Delta\hat{\tau}_2$ are affected by the charge and the bounce parameter.

In a summary, both the charge and the bounce parameter affect the image positions, the magnification and the differential time delay of the lensed images starting from their first-order terms, while they change the total magnification and the centroid beginning from their second-order terms. Therefore, it would be easier to distinguish the black-bounce-Reissner–Nordström spacetime from the Schwarzschild black hole by measuring the image positions, the magnification and the differential time delay. This circumstance is also true for other tidal/charged spacetimes, such as the Reissner–Nordström black hole, the tidal Reissner–Nordström black hole, the charged Horndeski black hole and the charged Galileon black hole, so that it would be necessary to assess the possibility of telling difference among these spacetimes by the weak deflection gravitational lensing alone.

3.6 Practical observables

In astronomical observations, the practical observables of the weak deflection gravitational lensing contain the angular separation P_{tot}, the difference of the angular positions ΔP, the total flux F_{tot}, the difference of the fluxes ΔF, the centroid S_{cent} and the differential time delay $\Delta \tau$ of the lensed images [50]. These practical observables can be found from the scaled quantities $(\beta, \theta, \mu, \hat{\tau})$, in which the observed flux is the magnified one of the unlensed source, i.e., $F = |\mu| F_{src}$. Keeping the leading contributions of the charge and the bounce parameter, we find the practical observables of the weak deflection gravitational lensing by the black-bounce-Reissner–Nordström spacetime as

$$P_{tot} = \vartheta^+ + \vartheta^-, \tag{68}$$

$$\Delta P = \vartheta^+ - \vartheta^-, \tag{69}$$

$$F_{tot} = F^+ + F^-, \tag{70}$$

$$\Delta F = F^+ - F^-, \tag{71}$$

$$S_{cent} = \frac{\vartheta^+ F^+ - \vartheta^- F^-}{F_{tot}}, \tag{72}$$

$$\Delta \tau = \tau^+ - \tau^-. \tag{73}$$

In order to demonstrate the effects of the charge and the bounce parameter on these observables in the weak deflection gravitational lensing, their deviations from those of the Schwarzschild black hole are defined as

$$\delta P_{tot} \equiv P_{tot} - P_{tot}(q = l = 0), \tag{74}$$

$$\delta \Delta P \equiv \Delta P - \Delta P(q = l = 0), \tag{75}$$

$$\delta r_{tot} \equiv 2.5 \log_{10} \left[\frac{F_{tot}}{F_{tot}(q = l = 0)} \right], \tag{76}$$

$$\delta \Delta r \equiv 2.5 \log_{10} \left[\frac{\Delta F}{\Delta F(q = l = 0)} \right], \tag{77}$$

$$\delta S_{cent} \equiv S_{cent} - S_{cent}(q = l = 0), \tag{78}$$

$$\delta \Delta \tau \equiv \Delta \tau - \Delta \tau(q = l = 0). \tag{79}$$

Here, δr_{tot} and $\delta \Delta r$, which are related to the fluxes, are transformed into the magnitude of brightness according to the astronomical convention. We find that the charge and the bounce parameter appear in the first-order terms of P_{tot}, ΔP, ΔF and $\Delta \tau$, while they only affect the second-order terms of F_{tot} and S_{cent}. It means that the deviations δr_{tot} and δS_{cent} would be much more difficult to detect than others and they would be unreachable with current techniques.

3.7 Example of Sgr A*

We take the supermassive black hole, Sgr A*, as the lens with the mass $m_{\bullet, SgrA*} = 4.28 \times 10^6\ M_\odot$ and the distance $D_{OL, SgrA*} = 8.32$ kpc [110]. Considering that the star S175 orbiting Sgr A* has the periastron distance of 2×10^{-4} pc

[110], we assume a luminous source with a distance to Sgr A* as $D_{LS} = 10^{-3}$ pc. Since the observables in the weak deflection gravitational lensing depend on two physical parameters, which are the charge q and the bounce parameter l, and one geometric parameter, which is the (dimensionless) angular position of the source β, we adopt three following domains to evaluate these observables

$$\mathcal{D}_\lambda = \{(\beta, q, \lambda) | 10^{-2} \leq \beta \leq 10,\ 0 \leq q \leq 1,\ \lambda = 0.5\}, \tag{80}$$

$$\mathcal{D}_q = \{(\beta, q, \lambda) | 10^{-2} \leq \beta \leq 10,\ q = 0.5,\ 0 \leq \lambda \leq 1\}, \tag{81}$$

$$\mathcal{D}_\beta = \{(\beta, q, \lambda) | \beta = 0.5,\ 0 \leq q \leq 1,\ 0 \leq \lambda \leq 1\}, \tag{82}$$

where the rescaled bounce parameter λ relates to the dimensionless one l via Eq. (7).

From top to bottom, Fig. 2 shows the angular separation between the two lensed images P_{tot}, its deviation from the one of the Schwarzschild black hole δP_{tot}, the difference of the angular positions of the two lensed images ΔP and its deviation from the one of the Schwarzschild black hole $\delta \Delta P$ on the domains of $\mathcal{D}_\lambda$, $\mathcal{D}_q$ and $\mathcal{D}_\beta$ (from left to right). The dash-dotted lines mark the upper bound on q based on the shadow of M87* observed by EHT, see Eq. (10). On $\mathcal{D}_\lambda$ and $\mathcal{D}_q$ shown in Fig. 2a, b, P_{tot} ranges from about 1.1 to 5.7 milliarcsecond (mas) and grows with the angular position of the source β, but barely changes with the charge q on $\mathcal{D}_\lambda$ and with the rescaled bounce parameter λ on $\mathcal{D}_q$. On $\mathcal{D}_\beta$ shown in Fig. 2c, it varies from about 1.155 to 1.162 mas and increases with the growth of λ and with the decline of q. With about 3 mas angular resolution of GRAVITY [106], it would be possible to measure P_{tot} if β and λ are sufficiently big and q is small enough. In Fig. 2d–f, δP_{tot} ranges from about -3.0 to 2.0 microarcsecond (μas) on $\mathcal{D}_\lambda$, from about -1.7 to 1.4 μas on $\mathcal{D}_q$, and from about -3.1 to 3.9 μas on $\mathcal{D}_\beta$. It decreases with q and increases with λ, but is hardly influenced by β. Below about 10–20 μas astrometric accuracy for GRAVITY [106], δP_{tot} would be impossible to detect so that one might not be able to distinguish the black-bounce-Reissner–Nordström spacetime from the Schwarzschild black hole by it. On $\mathcal{D}_\lambda$ and $\mathcal{D}_q$ shown in Fig. 2g, h, ΔP ranges from about 0 to 5.5 mas and increases with β, but barely varies with q on $\mathcal{D}_\lambda$ and with λ on $\mathcal{D}_q$. On $\mathcal{D}_\beta$ shown in Fig. 2i, it varies from about 272.4 to 274.1 μas and increases with q and with the decrease of λ. When β and q are big enough and λ is sufficiently small, it might be possible to measure ΔP by GRAVITY. Based on Fig. 2j–l, $\delta \Delta P$ changes from about -1.6 to 3.0 μas on $\mathcal{D}_\lambda$, from about -1.0 to 1.6 μas on $\mathcal{D}_q$, and from about -1.0 to 0.7 μas on $\mathcal{D}_\beta$. When $\beta \gtrsim 0.5$, $\delta \Delta P$ would be distinctly grows with q and decreases with λ; otherwise, it barely affected by q on $\mathcal{D}_\lambda$ and by λ on $\mathcal{D}_q$. Since GRAVITY does not have enough astrometric accuracy to detect $\delta \Delta P$, it would be infeasible

to distinguish the black-bounce-Reissner–Nordström spacetime from the Schwarzschild black hole by this observable.

Figure 3 shows the total flux of the two lensed images F_{tot}, its deviation from the one of the Schwarzschild black hole δr_{tot}, the difference of the fluxes of the two lensed images ΔF and its deviation from the one of the Schwarzschild black hole $\delta \Delta r$ on the domains of $\mathcal{D}_\lambda$, $\mathcal{D}_q$ and $\mathcal{D}_\beta$. On $\mathcal{D}_\lambda$ and $\mathcal{D}_q$ displayed in Fig. 3a, b, the normalized total flux $F_{\text{tot}}/F_{\text{src}}$ ranges from about 1 to 100 and it decreases with β, but barely changes with q on $\mathcal{D}_\lambda$ and with λ on $\mathcal{D}_q$. On $\mathcal{D}_\beta$ displayed in Fig. 3c, it stays at the level of 2.182 and grows with q and λ. When $\beta \lesssim 0.5$, the total flux of the two lensed images can be magnified nearly by a factor of 100, which might be easily observed if the unlensed flux of the source F_{src} itself is bright enough. In Fig. 3d–f, δr_{tot} changes from about 0 to 8×10^{-5} mag on $\mathcal{D}_\lambda$, from about 0 to 6×10^{-5} mag on $\mathcal{D}_q$, and from about 0 to 7×10^{-5} mag on $\mathcal{D}_\beta$. When $\beta \lesssim 1$, δr_{tot} increases with q and λ; otherwise, it hardly affected by them. Such a small level of δr_{tot} is far beyond the current ability of photometry, even for a dedicated space-bone satellite with photometric resolution of about 300 parts per million or 3.2×10^{-4} mag [111]. On $\mathcal{D}_\lambda$ and $\mathcal{D}_q$ displayed in Fig. 3g, h, $\Delta F/F_{\text{src}} - 1$ ranges from about -7.5×10^{-3} to 0 and it increases with β, but stays almost unchanged with q on $\mathcal{D}_\lambda$ and with λ on $\mathcal{D}_q$. On $\mathcal{D}_\beta$ displayed in Fig. 3i, it varies from about -8×10^{-3} to -5×10^{-3} and increases with q and with the decline of λ. Such a brightness difference is reachable by a space telescope [111]. According to Fig. 3j–l, $\delta \Delta r$ changes from about -10^{-3} to 10^{-3} mag on $\mathcal{D}_\lambda$, from about -7×10^{-4} to 7×10^{-4} mag on $\mathcal{D}_q$, and from about -1.8×10^{-3} to 1.3×10^{-3} mag on $\mathcal{D}_\beta$. When $\beta \lesssim 1$, $\delta \Delta r$ would be distinctly grows with q and decreases with λ; otherwise, it is barely varied by q on $\mathcal{D}_\lambda$ and by λ on $\mathcal{D}_q$. Since $\delta \Delta r$ is mostly within the photometric resolution of a dedicated space mission [111], it might be possible to distinguish the black-bounce-Reissner–Nordström spacetime from the Schwarzschild black hole by measuring $\delta \Delta r$; however, flares of Sgr A* might wipe out any brightness difference.

Figure 4 shows the centroid of the lensed images S_{cent}, its deviation from the one of the Schwarzschild black hole δS_{cent}, the differential time delay between the lensed images $\Delta \tau$ and its deviation from the one of the Schwarzschild black hole $\delta \Delta \tau$ on the domains of $\mathcal{D}_\lambda$, $\mathcal{D}_q$ and $\mathcal{D}_\beta$ (from left to right). On $\mathcal{D}_\lambda$ and $\mathcal{D}_q$ demonstrated in Fig. 4a, b, S_{cent} ranges from about 0 to 6 mas and grows with β, but barely changes with q on $\mathcal{D}_\lambda$ and with λ on $\mathcal{D}_q$. On $\mathcal{D}_\beta$ shown in Fig. 4c, it stays at the level of 400 μas and decreases with q and λ. When $\beta \sim 10$, it would be possible for GRAVITY to marginally detect S_{cent}. In Fig. 4d–f, δS_{cent} ranges from about -21 to 0 nanoarcsecond (nas) on $\mathcal{D}_\lambda$, from about -12 to 0 nas on $\mathcal{D}_q$, and from about -17 to 0 nas on $\mathcal{D}_\beta$. When $\beta \sim 1$, δS_{cent} might have its biggest deviations as $q \sim 1$ and $\lambda \sim 1$. However, it would still be too small to measure in the foreseen

future. On $\mathcal{D}_\lambda$ and $\mathcal{D}_q$ shown in Fig. 4g, h, $\Delta \tau$ ranges from about 0.03 to 76 min and increases with β, but barely changes with q on $\mathcal{D}_\lambda$ and with λ on $\mathcal{D}_q$. On $\mathcal{D}_\beta$ shown in Fig. 4i, it varies from about 85.9 to 86.5 min and increases with λ and with the decrease of q. Since typical datasets of Sgr A* and S2 star by GRAVITY contains exposures with an individual integration time of 10 s, $\Delta \tau$ might be measurable if it can reach the level longer than a few minutes. Based on Fig. 4j–l, $\delta \Delta \tau$ changes from about -4.2 to 2.6 s on $\mathcal{D}_\lambda$, from about -2.4 to 1.5 s on $\mathcal{D}_q$, and from about -0.2 to 0.3 s on $\mathcal{D}_\beta$. When $\beta \sim 10$, $\delta \Delta \tau$ would be distinctly decreases with q and increases with λ; otherwise, it barely influenced by q on $\mathcal{D}_\lambda$ and by λ $\mathcal{D}_q$. Since the individual integration time of GRAVITY is longer than $\delta \Delta \tau$, it would be infeasible to distinguish the black-bounce-Reissner–Nordström spacetime from the Schwarzschild black hole by this observable.

As shown in Fig. 5, in order to indicate the differences in the lensing signatures and assess the possibility to distinguish various tidal or charged spacetimes, including the black-bounce-Reissner–Nordström spacetime, the Reissner–Nordström black hole, the tidal Reissner–Nordström black hole, the charged Horndeski black hole and the charged Galileon black hole, we compare their observables (left y-axes) and their deviations (right y-axes) from those of the Schwarzschild black hole in the case of $\beta = 0.5$. P_{tot} for all these spacetimes can reach the level of 1.1 mas, while its difference between them is no more than 10 μas, see Fig. 5a. Since such a tiny difference is beyond the current astrometric accuracy, it would be impossible to distinguish these spacetimes by measuring P_{tot}. Based on Fig. 5b, ΔP for these spacetimes stays at the level of 273 μas, but its difference between them is less than 2 μas, which is infeasible to detect by the present techniques of astrometry. Figure 5c shows that $F_{\text{tot}}/F_{\text{src}}$ for these spacetimes are at the level of 2.182, and the difference between them is smaller than 1.5×10^{-4} mag, which is unreachable for the current ability of photometry. Seen from Fig. 5d, we find that $\Delta F/F_{\text{src}} - 1$ ranges from -7.5×10^{-3} to -4.5×10^{-3} for various spacetimes. The difference between them can reach about a few 10^{-3} mag, which is within the capacity of a space-borne telescope. Moreover, as the increment of λ, the difference of ΔF between the black-bounce-Reissner–Nordström spacetime and other spacetimes can be enlarged, promising for distinguishing them. S_{cent} is at the level of about 400 μas for all of these spacetimes, while its difference between them does not exceed 40 nas as shown in Fig. 5e, which is far beyond the territory of current technology. $\Delta \tau$ for all these spacetimes is around 86 s, but its difference between them is no longer than 1 s as displayed in Fig. 5f, which is shorter than the integration time of an individual exposure in astronomical observation, making them indistinguishable.

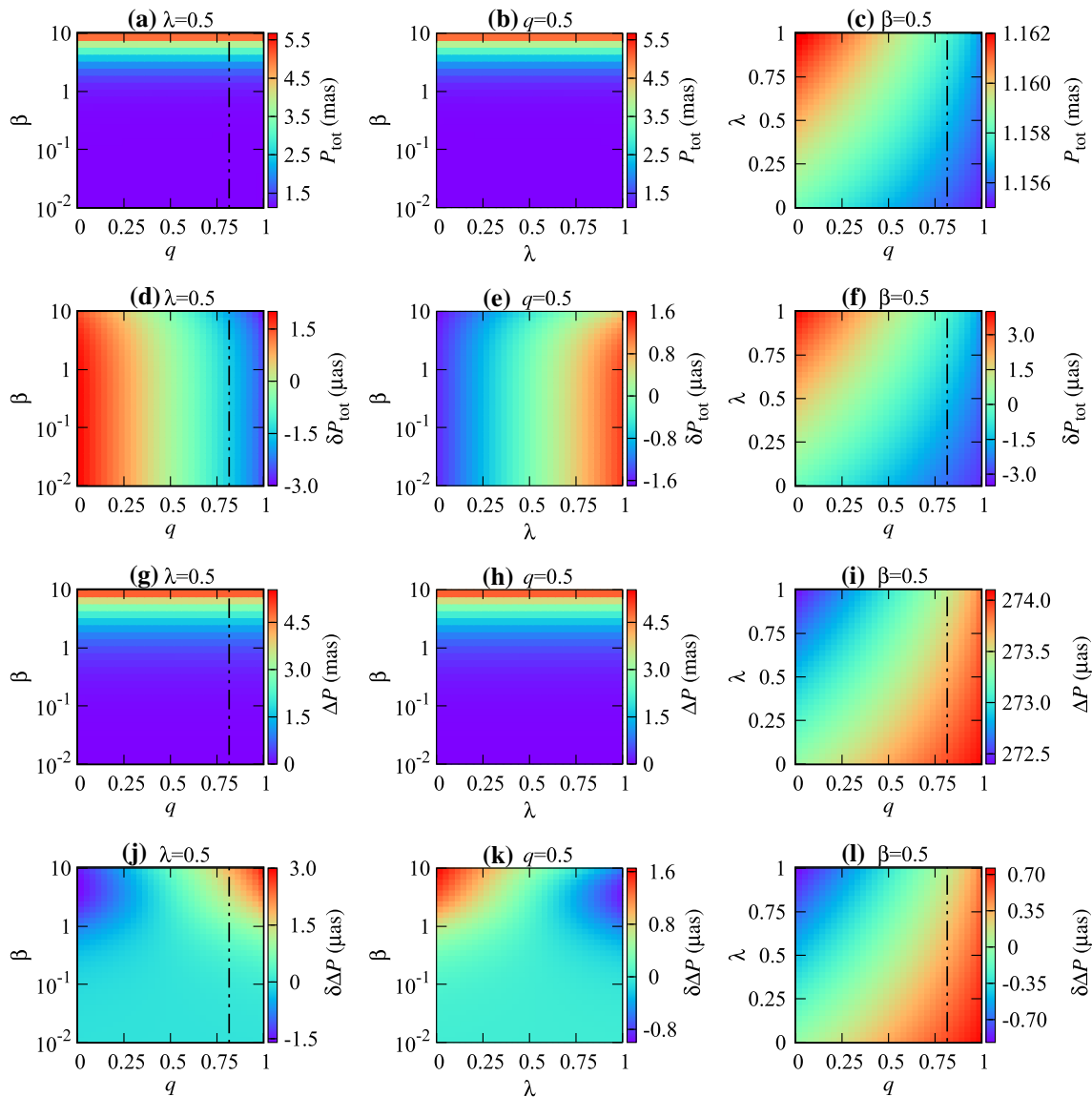In summary, we find that (1) the angular separation P_{tot}, the angular difference ΔP, the total flux F_{tot}, the fluxes dif-

Fig. 2 From top to bottom, color-indexed P_{tot}, δP_{tot}, ΔP and $\delta \Delta P$ in the weak deflection gravitational lensing for Sgr A* are shown on the domains of $\mathcal{D}_\lambda$, $\mathcal{D}_q$ and $\mathcal{D}_\beta$ (from left to right). The dash-dotted lines mark the upper bound on q based on the shadow of M87* observed by EHT (10)

ference ΔF, the centroid S_{cent} and the differential time delay $\Delta \tau$ are possible to detect with current technology; (2) it would be possible to distinguish the black-bounce-Reissner–Nordström spacetime from the Schwarzschild black hole, the Reissner–Nordström black hole, the tidal Reissner–Nordström black hole, the charged Horndeski black hole and the charged Galileon black hole by measuring $\delta \Delta r$ with a dedicated space-borne mission when Sgr A* is in its quiescence.

4 Strong deflection gravitational lensing

In the strong deflection gravitational lensing, the closest approach of the light ray to the black-bounce-Reissner–Nordström spacetime r_0 is at the same order of the gravitational radius of a compact object. As r_0 decreases to the radius of the photon sphere, the deflection angle of the photon will become divergent. This phenomenon can wind the light ray around the object before the photon reaches the observer, and, therefore, produce a set of relativistic images, which are absent in the weak deflection gravitational lensing.
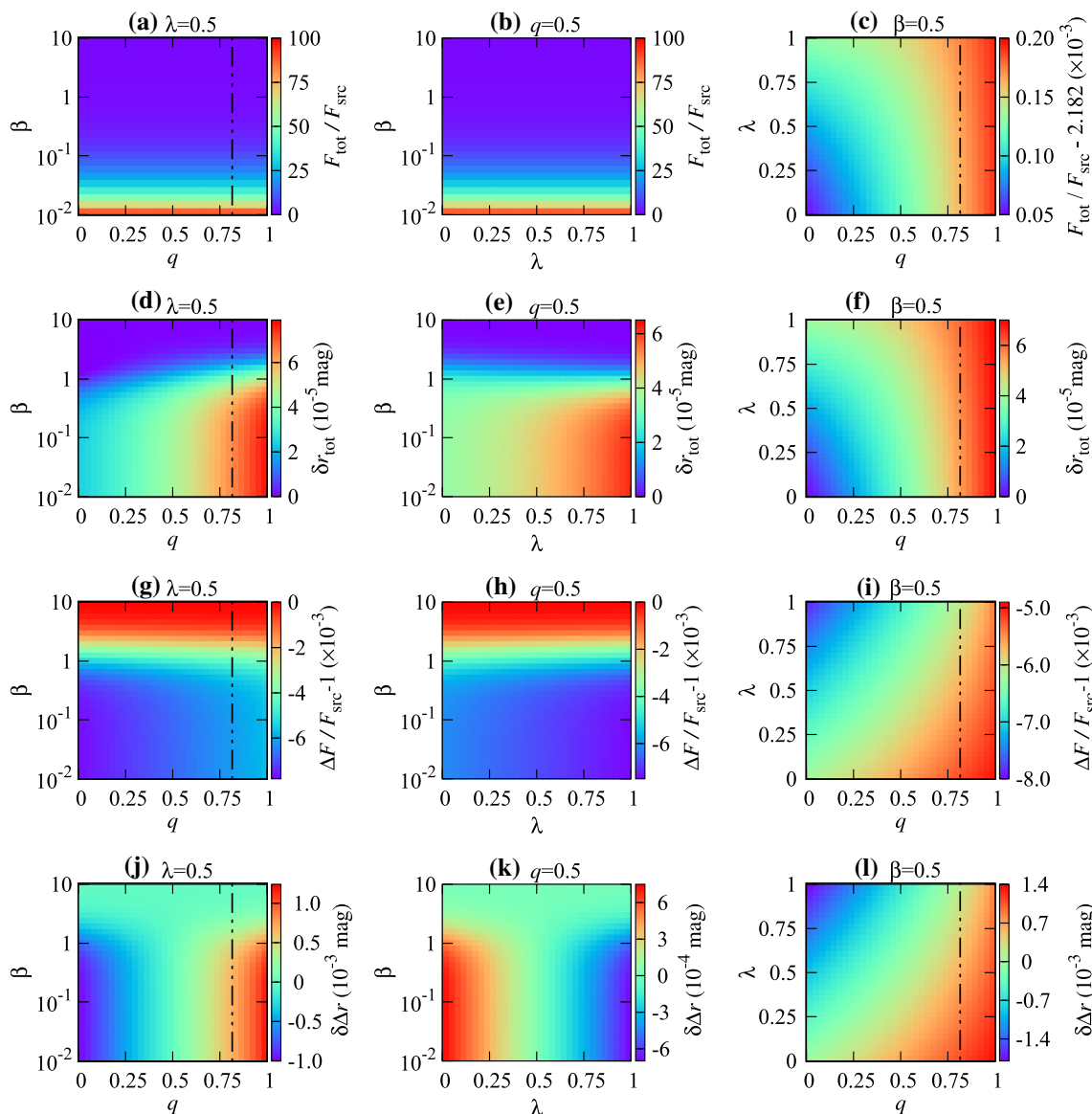
Fig. 3 From top to bottom, color-indexed F_{tot}, δr_{tot}, δr_{tot} and $\delta \Delta r$ in the weak deflection gravitational lensing for Sgr A* are shown on the domains of $\mathcal{D}_\lambda$, $\mathcal{D}_q$ and $\mathcal{D}_\beta$ (from left to right). The dash-dotted lines mark the upper bound on q based on the shadow of M87* observed by EH (10)

4.1 Photon sphere and shadow

As the unstable circular orbit of a photon for the black-bounce-Reissner–Nordström spacetime, the photon sphere has its radius r_m that is the biggest root to the following equation [55,112]

$$\frac{A'(r)}{A(r)} = \frac{C'(r)}{C(r)}, \tag{83}$$

where $'$ means the derivative against r, and we can have

$$r_m = \frac{1}{2}\sqrt{(3m_\bullet + \sqrt{9m_\bullet^2 - 8Q_\bullet^2})^2 - 4l_\bullet^2} \tag{84}$$

and its corresponding dimensionless one as

$$
\begin{aligned}
x_m &= \frac{r_m}{m_\bullet} \\
&= \frac{1}{2}\sqrt{(3 + \sqrt{9 - 8q})^2 - 4\lambda(1 + \sqrt{1 - q})^2},
\end{aligned}
\tag{85}
$$

where Eqs. (6) and (7) are used. The left panel of Fig. 6 represents that x_m decreases with the increment of q and λ. When both the dimensionless charge q and the rescaled bounce parameter λ are zeros, the photon sphere of the black-bounce-Reissner–Nordström spacetime will have its biggest radius with $x_m = 3$, which is the same as the one of the Schwarzschild black hole. As $q = \lambda = 1$, the spacetime (1) will has its smallest photon sphere with
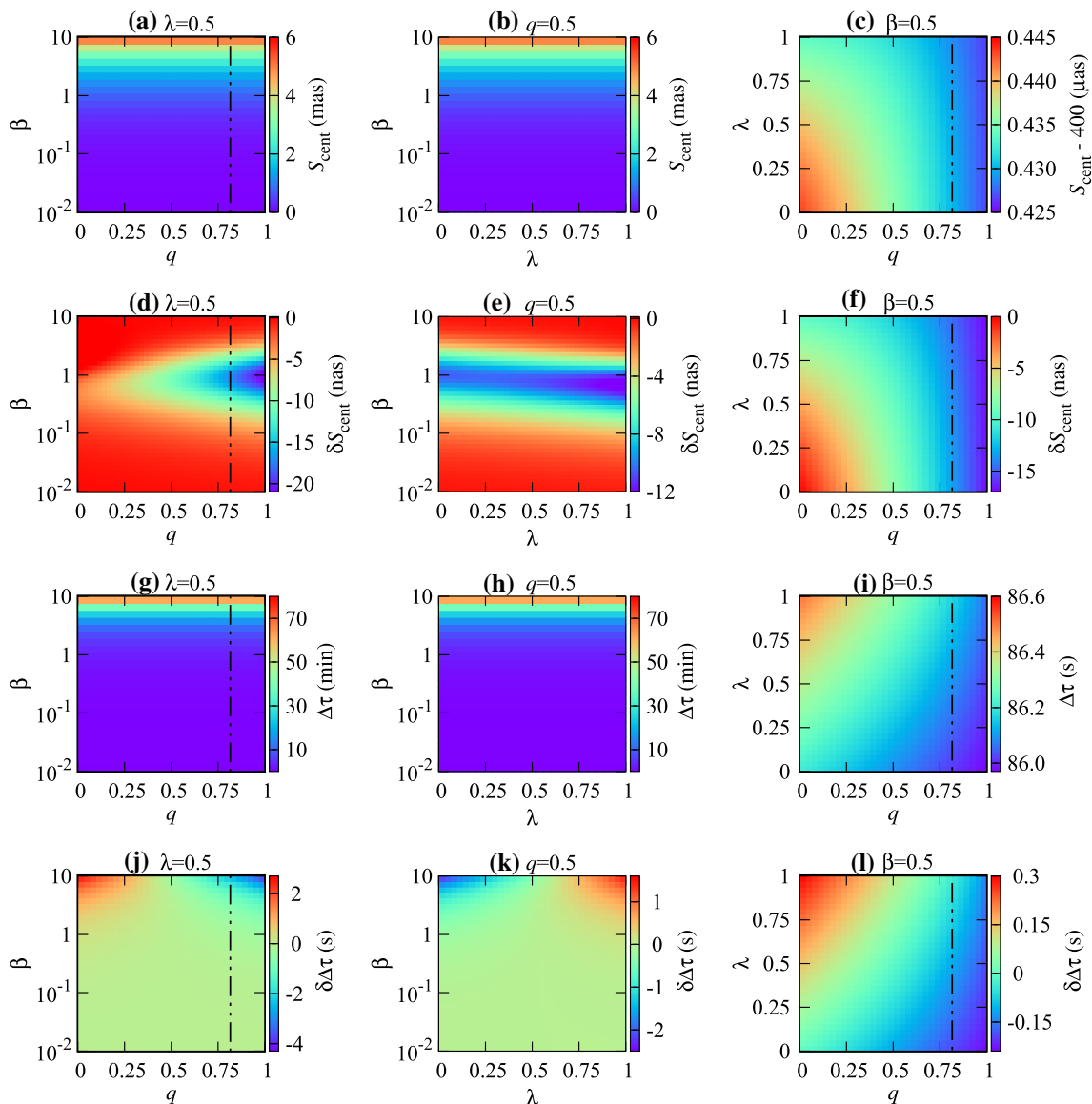
Fig. 4 From top to bottom, color-indexed S_{cent}, δS_{cent}, $\Delta\tau$ and $\delta\Delta\tau$ in the weak deflection gravitational lensing for Sgr A* are shown on the domains of $\mathcal{D}_\lambda$, $\mathcal{D}_q$ and $\mathcal{D}_\beta$ (from left to right). The dash-dotted lines mark the upper bound on q based on the shadow of M87* observed by EHT (10)

$x_{\rm m} = \sqrt{3}$. The right panel of Fig. 6 displays a comparison of $x_{\rm m}$ with respect to q for the black-bounce-Reissner–Nordström spacetime, the Reissner–Nordström black hole, the tidal Reissner–Nordström black hole, the charged Horndeski black hole and the charged Galileon black hole, among which the Reissner–Nordström black hole and the charged Galileon black hole share the same $x_{\rm m}$. As the growth of q, $x_{\rm m}$ shrinks for all the spacetimes. For a given q, the photon sphere of the black-bounce-Reissner–Nordström spacetime is the smallest one, while a bigger rescaled bounce parameter λ renders $x_{\rm m}$ of the black-bounce-Reissner–Nordström spacetime even smaller than those of other black holes. The

tidal Reissner–Nordström black hole has the biggest photon sphere due to its negative tidal charge q.

Such a photon sphere can cast a shadow with the radius as

$$r_{\rm sh} = \sqrt{\frac{C_{\rm m}}{A_{\rm m}}}, \tag{86}$$

where and hereafter a subscript "m" denotes the value of a quantity at $r = r_{\rm m}$ and whose dimensionless version is

$$x_{\rm sh} = \frac{r_{\rm m}}{m_\bullet} = \frac{\sqrt{2}}{2}\frac{(3+\sqrt{9-8q})^{3/2}}{(1+\sqrt{9-8q})^{1/2}}. \tag{87}$$
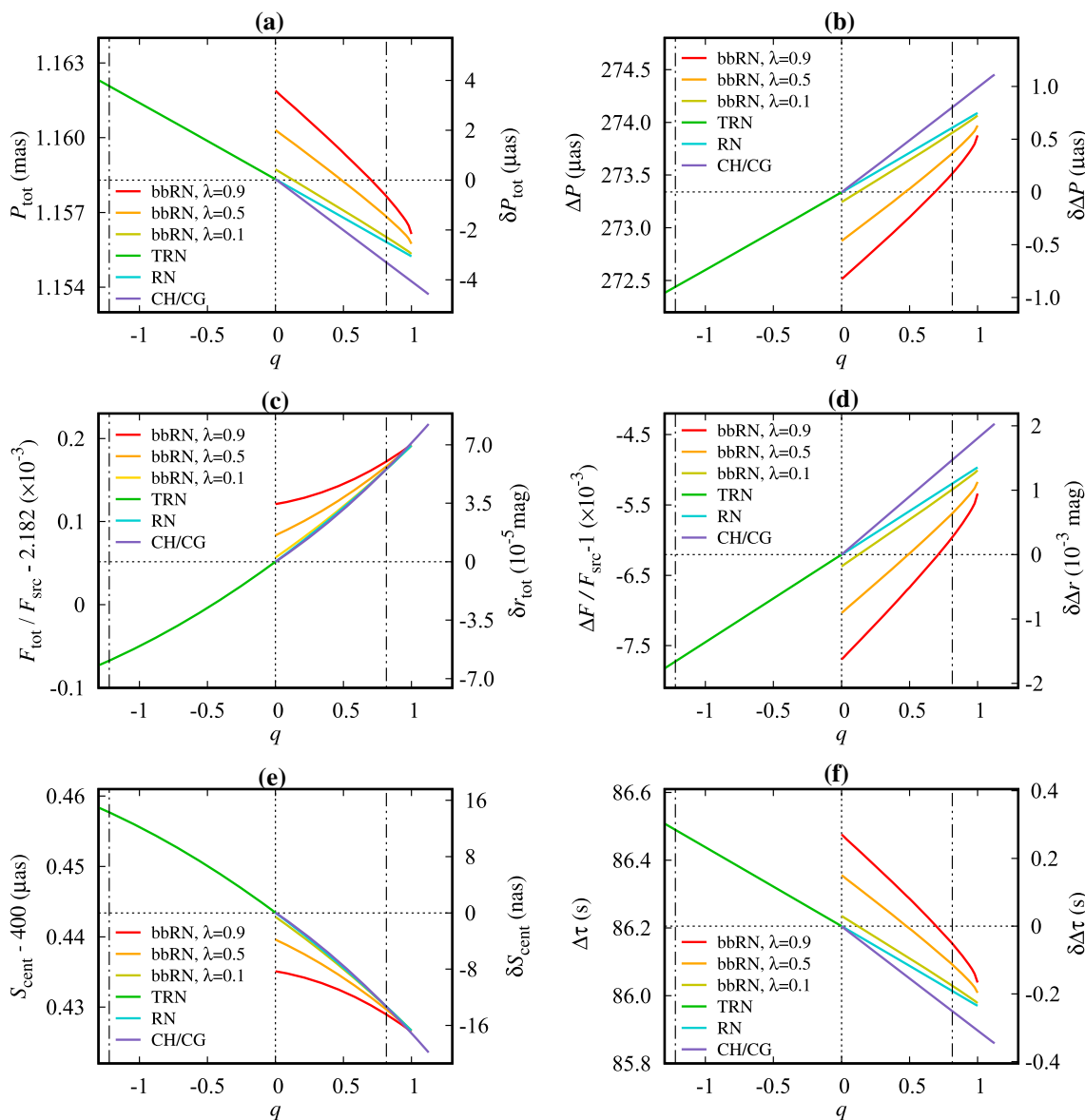
Fig. 5 Comparisons of the observables in the weak deflection gravitational lensing for Sgr A* by the black-bounce-Reissner–Nordström spacetime (bbRN), the Reissner–Nordström black hole (RN), the tidal Reissner–Nordström black hole (TRN), the charged Horndeski black hole (CH) and the charged Galileon black hole (CG) in the case of $\beta = 0.5$. The left and right dash-dotted lines mark the lower and upper bound on q based on the shadow of M87* observed by EHT, see Eqs. (10) and (11). The horizontal dotted lines denote those values for the Schwarzschild black hole

When the charge vanishes, i.e., $q = 0$, it returns to the one of the Schwarzschild black hole with $x_{\mathrm{sh,Sch}} = 3\sqrt{3}$. Figure 7 shows x_{sh} with respect to q for the black-bounce-Reissner–Nordström spacetime, the Reissner–Nordström black hole, the tidal Reissner–Nordström black hole, the charged Horndeski black hole and the charged Galileon black hole. All of x_{sh} declines as the increment of q. While the tidal Reissner–Nordström black hole has the biggest shadow due to its negative q, the charged Horndeski black hole has the smallest one since its q can reach 9/8. For a given q, the

black-bounce-Reissner–Nordström spacetime, the Reissner–Nordström black hole and the charged Galileon black hole share exactly the same x_{sh}, and the x_{sh} of the charged Horndeski black hole is very close to them numerically, making these four spacetimes indistinguishable based on the size of the shadow.

The size of the shadow of M87* measured by EHT is consistent with the prediction by general relativity within 17% at the 68-percentile level [107], paving the way for the strong-field tests of black holes and theories of gravitation. Applying

the scheme of Ref. [107] and using Eq. (86), the preliminary bounds on the dimensionless charge q for these spacetimes can be obtained according to the right y-axis and grey area in Fig. 7. We find that, for the black-bounce-Reissner–Nordström spacetime, the Reissner–Nordström black hole, the charged Horndeski black hole and the charged Galileon black hole, they have the same bound on q as

$$\mathcal{D} = \{q \mid 0 \leq q \leq 0.8144\},$$

while the bound for the tidal Reissner–Nordström black hole is

$$\mathcal{D}_{\text{TRN}} = \{q \mid -1.2198 \leq q \leq 0.8144\}.$$

It is necessary to address that we did not consider the effects of the spin of M87* and its inclination on the bounds on q. Since their effects on the size and the shape of M87*'s shadow are less than 4% and 7% respectively [113], it might be expected that the EHT measurement could be used to test these non-rotating tidal/charged spacetimes sufficiently and these bounds on the dimensionless charge q are valid at least for the leading order. For the physical (tidal) charge $Q_\bullet^2 = q\, m_\bullet^2$ of these spacetimes, they depend explicitly on the masses and would be different for various systems even for the same q.

4.2 Observables

Applying the method of the strong deflection limit [56], we can find the deflection angle in the strong deflection gravitational lensing as

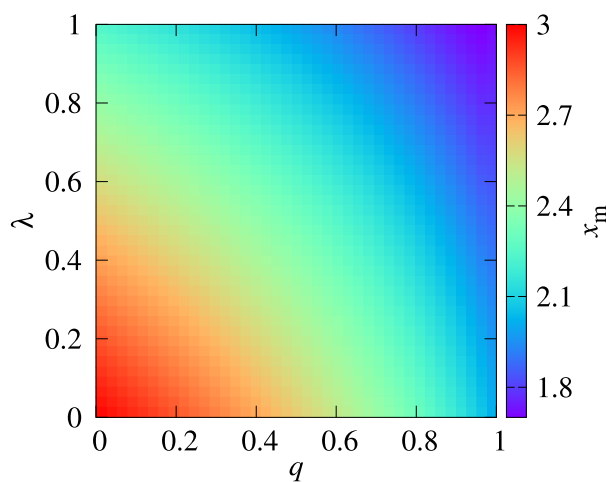$$\hat{\alpha}(\theta) = -\bar{a} \log\left(\frac{\theta D_{\text{OL}}}{u_m} - 1\right) + \bar{b}$$

$$+ \mathcal{O}[(u - u_m)\log(u - u_m)], \tag{88}$$

with

$$\bar{a} = \sqrt{\frac{2}{A_{\text{m}} C''_{\text{m}} - C_{\text{m}} A''_{\text{m}}}}, \tag{89}$$

$$\bar{b} = -\pi + \bar{a}\log\left[\frac{2C_{\text{m}}(1 - A_{\text{m}})^2}{\bar{a}^2 A_{\text{m}}^3 C_{\text{m}}'^2}\right]$$

$$+ 2\int_0^1 \left[\frac{(1 - A_{\text{m}})}{A'_z C_z}\left(\frac{A_{\text{m}}}{C_{\text{m}}} - \frac{A_z}{C_z}\right)^{-\frac{1}{2}} - \frac{\bar{a}}{z}\right]dz, \tag{90}$$

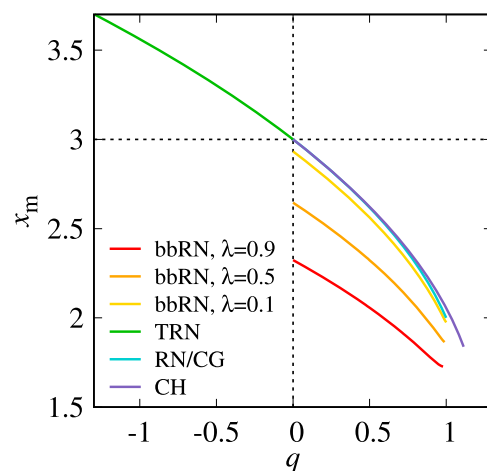where $A_z \equiv A[r(z)]$, $C_z \equiv C[r(z)]$, the variable z is defined as

$$z = \frac{A(r) - A_{\text{m}}}{1 - A_{\text{m}}}, \tag{91}$$

and u is the impact parameter, see Eq. (13).

Considering that both the observer and the source are distant from the lens and that the three of them are almost in a linear configuration, we can simplify the lens equation as [114]

$$\mathcal{B} = \vartheta - \frac{D_{\text{LS}}}{D_{\text{OS}}}(\hat{\alpha} - 2n\pi), \tag{92}$$

where n is the number of circles that the photon goes around the lens. Putting the deflection angle (88) into the lens equation (92), we can find the angular positions of the relativistic images. With the help of Eq. (16), the differential time delay between two relativistic images can be obtained as [115]

Fig. 6 Left panel: The dimensionless radius x_{m} of the photon sphere for the black-bounce-Reissner–Nordström spacetime with respect to q and λ. Right panel: A comparison of x_{m} among the black-bounce-Reissner–Nordström spacetime (bbRN), the Reissner–Nordström black hole (RN), the tidal Reissner–Nordström black hole (TRN), the charged Horndeski black hole (CH) and the charged Galileon black hole (CG)
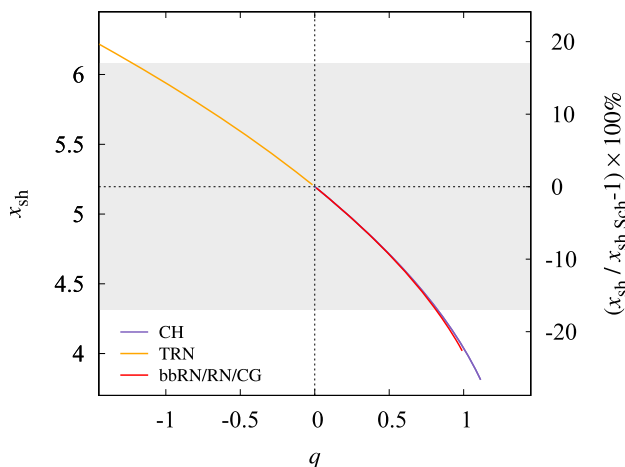
Fig. 7 The dimensionless radius x_{sh} (left y-axis) for the black-bounce-Reissner–Nordström spacetime (bbRN), the Reissner–Nordström black hole (RN), the tidal Reissner–Nordström black hole (TRN), the charged Horndeski black hole (CH) and the charged Galileon black hole (CG), and its relative deviation (right y-axis) from the one of the Schwarzschild black hole $x_{sh,Sch} = 3\sqrt{3}$. The grey area shows the allowed range of x_{sh} by the EHT measurement of M87*'s shadow

$$T_a - T_b = \tilde{T}(r_{0,a}) - \tilde{T}(r_{0,b}) + 2\int_{r_{0,a}}^{r_{0,b}} \frac{1}{A(r)} dr, \tag{93}$$

where $r_{0,a}$ and $r_{0,b}$ are the closest approaches of the photons for the relativistic images a and b, respectively, and the time function $\tilde{T}(r)$ is

$$\tilde{T} = -\tilde{a}\log\left(\frac{u}{u_m} - 1\right) + \tilde{b}$$
$$+ \mathcal{O}[(u - u_m)\log(u - u_m)], \tag{94}$$

with

$$\tilde{a} = \bar{a} u_m, \tag{95}$$

$$\tilde{b} = -\pi + \tilde{a}\log\left[\frac{(1 - A_m)^2}{A_m'^2}\left(\frac{C_m''}{C_m} - \frac{A_m''}{A_m}\right)\right]$$
$$+ 2\int_0^1\left\{\frac{(1 - A_m)\sqrt{A_m}}{A_z' A_z}\left[\left(1 - \frac{A_z C_m}{A_m C_z}\right)^{-\frac{1}{2}} - 1\right]\right.$$
$$\left. - \frac{\tilde{a}}{z}\right\} dz. \tag{96}$$

If one can resolve the first relativistic image ($n = 1$) only and see other images ($n \geq 2$) packed together, the observables in the strong deflection gravitational lensing can be found as the angular radius of the photon sphere (shadow) ϑ_∞, the angular separation s between the first relativistic image and the packed others and their magnitude difference Δm [56]

$$\vartheta_\infty = \frac{u_m}{D_{OL}}, \tag{97}$$

$$s = \theta_\infty \exp\left(\frac{\bar{b}}{\bar{a}} - \frac{2\pi}{\bar{a}}\right), \tag{98}$$

$$\Delta m = \frac{5\pi}{\bar{a}\log 10}. \tag{99}$$

If one can separate the first and second relativistic images, their differential time delay can be another observable as [115]

$$\Delta T_{2,1} = \Delta T_{2,1}^0 + \Delta T_{2,1}^1, \tag{100}$$

where the perimeter term $\Delta T_{2,1}^0$ and the exponential term $\Delta T_{2,1}^1$ are

$$\Delta T_{2,1}^0 = 2\pi u_m, \tag{101}$$

$$\Delta T_{2,1}^1 = 2\sqrt{2}\bar{a} u_m \exp\left(\frac{\bar{b}}{2\bar{a}}\right)$$
$$\times \left[\exp\left(-\frac{\pi}{\bar{a}}\right) - \exp\left(-\frac{2\pi}{\bar{a}}\right)\right]. \tag{102}$$

Since the perimeter term cannot provide information than u_m, we define the following ratio

$$\eta_{2,1} = \log_{10}\left(\frac{\Delta T_{2,1}^1}{\Delta T_{2,1}}\right), \tag{103}$$

to indicate the contribution of the exponential term to the total time delay. The deviations of these observables in the strong deflection gravitational lensing by the black-bounce-Reissner–Nordström spacetime from those of the Schwarzschild black hole can be obtained as

$$\delta\vartheta_\infty = \vartheta_\infty - \vartheta_\infty|_{q=l=0}, \tag{104}$$
$$\delta s = s - s|_{q=l=0}, \tag{105}$$
$$\delta\Delta m = \Delta m - \Delta m|_{q=l=0}, \tag{106}$$
$$\delta\Delta T_{2,1} = \Delta T_{2,1} - \Delta T_{2,1}|_{q=l=0}, \tag{107}$$
$$\delta\eta_{2,1} = \eta_{2,1} - \eta_{2,1}|_{q=l=0}. \tag{108}$$

4.3 Examples of Sgr A* and M87*

We take the supermassive black holes, Sgr A* and M87* as the lenses which have the following masses and distances $m_{\bullet,SgrA*} = 4.28 \times 10^6 \, M_\odot$, $D_{OL,SgrA*} = 8.32$ kpc [110] and $m_{\bullet,M87*} = 6.5 \times 10^9 \, M_\odot$, $D_{OL,M87*} = 16.8$ Mpc [12]. The observables in the strong deflection gravitational lensing will be estimated on the domain $\mathcal{D}_H$, see Eq. (8).

From top to bottom, Fig. 8 shows the angular radius of the photon sphere ϑ_∞, its deviation from the one of the Schwarzschild black hole $\delta\vartheta_\infty$, the angular separation s between the first relativistic image and the packed others, its deviation from the one of the Schwarzschild black hole δs, the magnitude difference between the first relativistic image and the packed others Δm and its deviation from the one of the Schwarzschild black hole $\delta\Delta m$. Since the observables have the same pattern for Sgr A* and M87*, one color bar with two specific scales and units (if necessary) is used. The dash-dotted lines mark the upper bound on q based on the
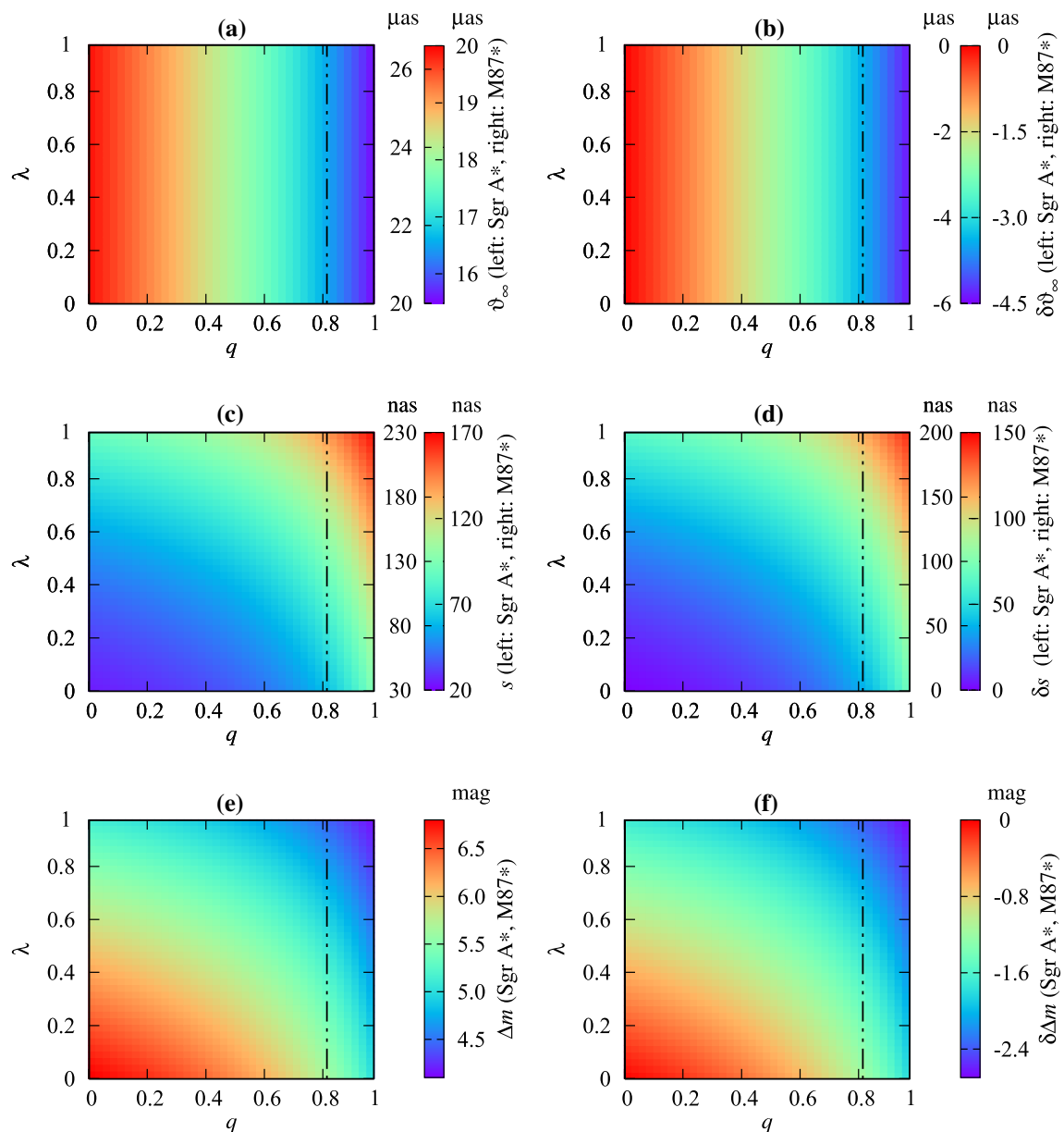
Fig. 8 Color-indexed $\vartheta_\infty, \delta\vartheta_\infty, s, \delta s, \Delta m$ and $\delta\Delta m$ in the strong deflection gravitational lensing are shown for Sgr A* and M87* on $\mathcal{D}_H$ (8). The dash-dotted lines mark the upper bound on q based on the shadow of M87* observed by EHT (10)

shadow of M87* observed by EHT (10). On $\mathcal{D}_H$ shown in Fig. 8a, b, ϑ_∞ ranges from about 20.7 to 26.6 µas for Sgr A* and from about 15.5 to 19.9 µas for M87*, while its deviation $\delta\vartheta_\infty$ varies from about −6.0 to 0 µas for Sgr A* and from about −4.4 to 0 µas for M87*. As shown in Sect. 4.1, ϑ_∞ and the resulting $\delta\vartheta_\infty$ are independent on λ and decrease with the charge q. Although the values of ϑ_∞ are within the ability of EHT, such a tiny $\delta\vartheta_\infty$ no more than 6 µas would be currently impossible to detect by EHT and one would not be able to distinguish the black-bounce-Reissner–Nordström spacetime from the Schwarzschild black hole by $\delta\vartheta_\infty$. Based on Fig. 8c, d, s ranges from about 33 to 225 nas for Sgr A*

and from about 25 to 168 nas, while its deviation δs changes from about 0 to 192 nas for Sgr A* and from about 0 to 143 nas for M87*. As q and λ increase, s and δs become bigger. Both s and δs are too small to resolve and detect for current technology. Figure 8e, f demonstrate that Δm ranges from about 4.1 to 6.8 mag and $\delta\Delta m$ changes from −2.7 to 0 mag. Since neither Δm nor $\delta\Delta m$ rely on the mass and the distance of the lens, Sgr A* and M87* share exactly the same these two observables. Both Δm and $\delta\Delta m$ are well within the current ability of photometry, whereas neither of them can be detected due to the fact that the angular separation of the first relativistic image s is too tiny to resolve.
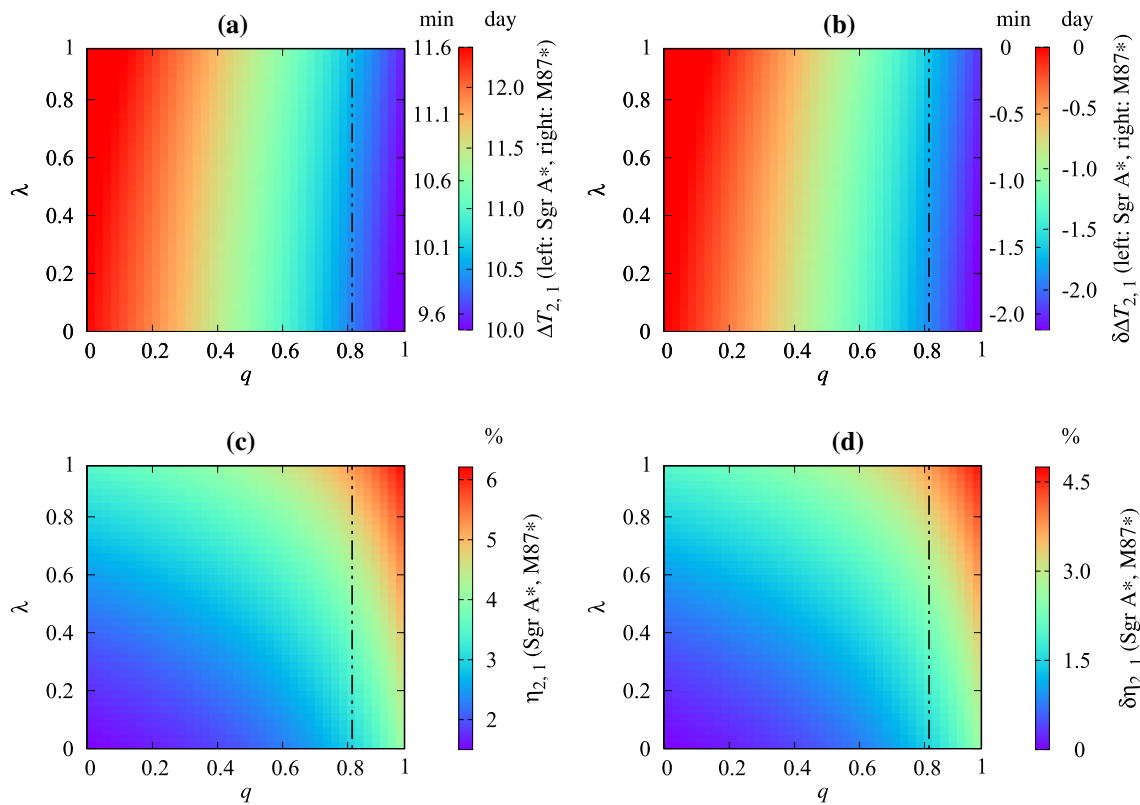
Fig. 9 Color-indexed $\Delta T_{2,1}$, $\delta\Delta T_{2,1}$, $\eta_{2,1}$ and $\delta\eta_{2,1}$ in the strong deflection gravitational lensing are shown for Sgr A* and M87* on $\mathcal{D}_H$ (8). The dash-dotted lines mark the upper bound on q based on the shadow of M87* observed by EHT (10)

Figure 9 shows the differential time delay between the first and second relativistic images $\Delta T_{2,1}$, its deviation from the one of the Schwarzschild black hole $\delta\Delta T_{2,1}$, the ratio of the exponential term to the total time delay $\eta_{2,1}$ and its deviation from the one of the Schwarzschild black hole $\delta\eta_{2,1}$. From Fig. 9a, b, it can be seen that $\Delta T_{2,1}$ ranges from about 9.3 to 11.8 min for Sgr A* and from about 9.9 to 12.6 days for M87*, while its deviation $\delta\Delta T_{2,1}$ can reach −2.6 min for Sgr A* and −2.7 days for M87*. The values of $\Delta T_{2,1}$ and $\delta\Delta T_{2,1}$ for M87* are within the current ability, but the inseparableness of the first and second relativistic images makes them unreachable. Figure 9c, d display that $\eta_{2,1}$ ranges from about 1.5 to 6.2% and $\delta\eta_{2,1}$ changes from 0 to 4.6% for both Sgr A* and M87* because $\eta_{2,1}$ and $\delta\eta_{2,1}$ are independent on the mass and the distance of the lens. Like the case of the differential time delay, they are inaccessible as well due to the tiny separation between the first and second relativistic images.

In order to indicate the differences in the signatures of the strong deflection gravitational lensing and evaluate the possibility to distinguish these tidal/charged spacetimes, we compare the observables for Sgr A* (left y-axes) and M87* (right y-axes) by the black-bounce-Reissner–Nordström spacetime, the Reissner–Nordström black hole, the tidal Reissner–Nordström black hole, the charged Horndeski black hole and

the charged Galileon black hole as shown in Fig. 10. The left and right dash-dotted lines mark the lower and upper bound on q based on the shadow of M87* observed by EHT, see Eqs. (10) and (11). ϑ_∞ for all these spacetimes can reach the level of about 20–30 μas, while its difference between them is no more than 10 μas, see Fig. 10a. In fact, the black-bounce-Reissner–Nordström spacetime, the Reissner–Nordström black hole, the charged Horndeski black hole and the charged Galileon black hole have nearly identical ϑ_∞ for a given q, making them effectively indistinguishable. Although the tidal Reissner–Nordström black hole can have a bigger ϑ_∞ due to its negative charge, such a difference is still beyond the ability of EHT. Based on Fig. 10b, s for these spacetimes and its difference between them for a given q are less than 200 nas and a few tens of nas, respectively, both of which are impossible to reach for the present techniques. Figure 10c shows that Δm for these spacetimes are at the level of several mag, and the difference between them is smaller than 1 mag. Due to the inseparability of the first and second relativistic images, it is infeasible to distinguish these spacetimes by measuring it. Seen from Fig. 10d, we find that $\Delta T_{2,1}$ for these spacetimes can reach about 15 min for Sgr A* and about 15 days for M87*. The difference among the black-bounce-Reissner–Nordström spacetime, the Reissner–Nordström black hole, the charged Horndeski black hole and
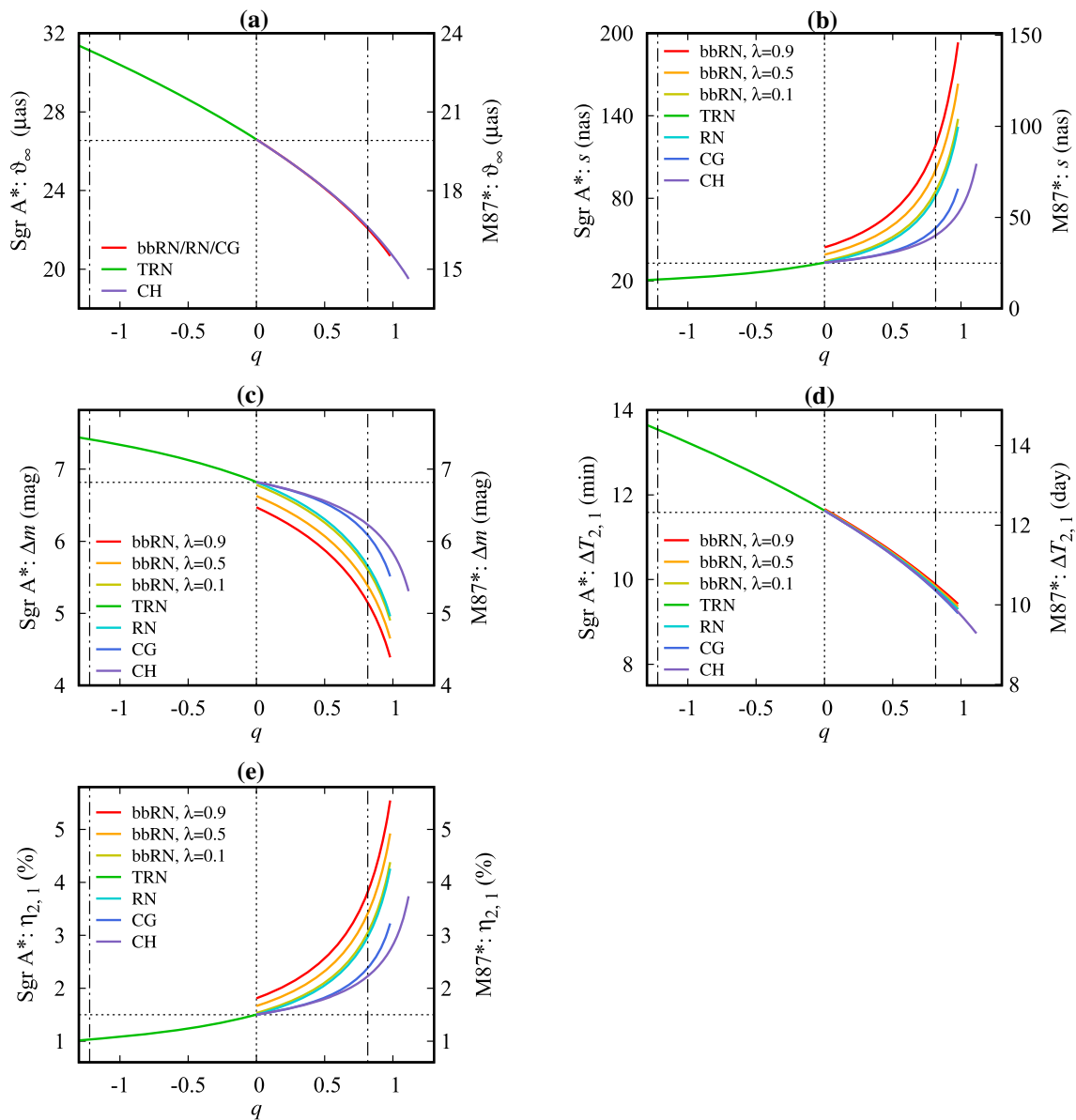
Fig. 10 Comparisons of the observables in the strong deflection gravitational lensing for Sgr A* (left y-axes) and M87* (right y-axes) by the black-bounce-Reissner–Nordström spacetime (bbRN), the Reissner–Nordström black hole (RN), the tidal Reissner–Nordström black hole (TRN), the charged Horndeski black hole (CH) and the charged Galileon black hole (CG). The left and right dash-dotted lines mark the lower and upper bound on q based on the shadow of M87* observed by EHT, see Eqs. (10) and (11). The horizontal dotted lines denote those values for the Schwarzschild black hole

charged Galileon black hole for a given q is too tiny to tell. According to Fig. 10e, $\eta_{2,1}$ for all these spacetimes is no more than 6.2%, and its difference between them for a given q is less than about 2%. Since it is unable to resolve the first and second relativistic images, neither $\Delta T_{2,1}$ nor $\eta_{2,1}$ can be used to distinguish these spacetimes.

In summary, we find that (1) it is possible to observe the apparent size of the photon sphere ϑ_∞; (2) it is impossible for the current ability to detect any other observables in the strong deflection gravitational lensing due to

exceedingly small separation of the first and second relativistic images; and (3) it is also impossible to distinguish the black-bounce-Reissner–Nordström spacetime from the Schwarzschild black hole, the Reissner–Nordström black hole, the tidal Reissner–Nordström black hole, the charged Horndeski black hole and the charged Galileon black hole by measuring observables in the strong deflection gravitational lensing by Sgr A* and M87*.

5 Conclusions and discussion

In this work, we investigate the weak and strong deflection gravitational lensing by the black-bounce-Reissner–Nordström spacetime. For the scenario of the weak deflection gravitational lensing, we find its lensing observables, such as the angular positions, magnification and time delay of the two lensed images. Taking Sgr A* as the lens, we assess their observability and show that it is possible to measure the angular separation, the angular difference, the fluxes difference, the centroid and the differential time delay between the lensed images with current techniques. The black-bounce-Reissner–Nordström spacetime might be distinguished from the Schwarzschild black hole, the Reissner–Nordström black hole, the tidal Reissner–Nordström black hole, the charged Horndeski black hole and the charged Galileon black hole by measuring the fluxes difference with a dedicated space telescope as long as Sgr A* is in its quiescence. For the case of the strong deflection gravitational lensing, we work out its observables, for instance the apparent radius of the photon sphere, the angular separation and the brightness difference between the first and the packed other images, and the differential time delay between the first and second relativistic images. Using Sgr A* and M87* as the lenses, we evaluate the possibility for measuring these observables and detecting their deviations from those of the Schwarzschild black hole. We demonstrate that it is possible to measure the apparent size of the photon sphere. However, other observables and all of the deviations are far beyond the reach of current technology. We also find that it is infeasible to distinguish the black-bounce-Reissner–Nordström spacetime from the Schwarzschild black hole, the Reissner–Nordström black hole, the tidal Reissner–Nordström black hole, the charged Horndeski black hole and the charged Galileon black hole by the strong deflection gravitational lensing of Sgr A* and M87*; even so, we still obtain preliminary bounds on the (dimensionless) charge based on the apparent size of M87*'s photon sphere observed by EHT: $0 \leq q \leq 0.8144$ for the black-bounce-Reissner–Nordström spacetime, the Reissner–Nordström black hole, the charged Horndeski black hole and the charged Galileon black hole and $-1.2198 \leq q \leq 0.8144$ for the tidal Reissner–Nordström black hole.

Black holes are rotating and moving in the real Universe. The EHT's observation disfavors a non-rotating M87* [7]. As an extension of the black-bounce-Reissner–Nordström spacetime by including the spin, the black-bounce-Kerr–Newman spacetime can be interpreted as charged dust with a nonlinear electrodynamics, or as Maxwell electrodynamics with an anisotropic fluid [38,116]. A study on its gravitational lensing will be our next move. Before proceeding, we might make a well-educated guess that its gravitational-lensing characters would be distinctly different from those given in this work because its spin might shift and distort the caustic, which is already known in other cases [117–135]. Moreover, the interpretation of the EHT's observation on M87* relies heavily on the general relativistic magneto-hydrodynamics of plasma around the Kerr black hole [11] with many untested assumptions about accretion flow and emission physics [136]. It is hardly possible to tell whether any detected deviation would become from a new space-time or from the violation of these astrophysical assumptions. Although very challenging space-based interferometry would be demanded [137–139], the photon ring [140] around M87* might provide a more robust test. Therefore, we have to admit that we might not be able to constrain the black-bounce-Reissner–Nordström spacetime and other tidal/charged spacetimes based on the M87*'s photon sphere self-consistently in the current stage, but the preliminary bounds on them we given in this work might still be valid at the leading order. Considering that it would not be easy to distinguish the black-bounce-Reissner–Nordström spacetime from the Schwarzschild black hole and other various spacetimes, the timelike geodesic motions around it, such as precessing [141–147] and periodic [148–160] orbits, might be another important way to understand and test it.

Data Availability Statement This manuscript has no associated data or the data will not be deposited. [Authors' comment: This paper is a theoretical work and all of the data are adopted by the related references.]

References

1. B.P. Abbott et al. (LIGO Scientific and Virgo Collaborations), Phys. Rev. Lett. **116**(6), 061102 (2016). https://doi.org/10.1103/PhysRevLett.116.061102
2. B.P. Abbott et al. (LIGO Scientific and Virgo Collaborations), Phys. Rev. X **6**(4), 041015 (2016). https://doi.org/10.1103/PhysRevX.6.041015
3. B.P. Abbott et al. (LIGO Scientific and Virgo Collaborations), Phys. Rev. Lett. **116**(24), 241103 (2016). https://doi.org/10.1103/PhysRevLett.116.241103

4. B.P. Abbott et al. (LIGO Scientific and Virgo Collaborations), Phys. Rev. Lett. **118**(22), 221101 (2017). https://doi.org/10.1103/PhysRevLett.118.221101

5. B.P. Abbott et al. (LIGO Scientific and Virgo Collaborations), Astrophys. J. Lett. **851**, L35 (2017). https://doi.org/10.3847/2041-8213/aa9f0c

6. B.P. Abbott et al. (LIGO Scientific and Virgo Collaborations), Phys. Rev. Lett. **119**(14), 141101 (2017). https://doi.org/10.1103/PhysRevLett.119.141101

7. K. Akiyama et al. (Event Horizon Telescope Collaboration), Astrophys. J. Lett. **875**, L1 (2019). https://doi.org/10.3847/2041-8213/ab0ec7

8. K. Akiyama et al. (Event Horizon Telescope Collaboration), Astrophys. J. Lett. **875**, L2 (2019). https://doi.org/10.3847/2041-8213/ab0c96

9. K. Akiyama et al. (Event Horizon Telescope Collaboration), Astrophys. J. Lett. **875**, L3 (2019). https://doi.org/10.3847/2041-8213/ab0c57

10. K. Akiyama et al. (Event Horizon Telescope Collaboration), Astrophys. J. Lett. **875**, L4 (2019). https://doi.org/10.3847/2041-8213/ab0e85

11. K. Akiyama et al. (Event Horizon Telescope Collaboration), Astrophys. J. Lett. **875**, L5 (2019). https://doi.org/10.3847/2041-8213/ab0f43

12. K. Akiyama et al. (Event Horizon Telescope Collaboration), Astrophys. J. Lett. **875**, L6 (2019). https://doi.org/10.3847/2041-8213/ab1141

13. J. Bardeen, in *Proceedings of International Conference GR5* (Tbilisi University Press, Tbilisi, USSR, 1968), p. 174

14. S.A. Hayward, Phys. Rev. Lett. **96**(3), 031103 (2006). https://doi.org/10.1103/PhysRevLett.96.031103

15. C. Bejarano, G.J. Olmo, D. Rubiera-Garcia, Phys. Rev. D **95**(6), 064043 (2017). https://doi.org/10.1103/PhysRevD.95.064043

16. C.C. Menchon, G.J. Olmo, D. Rubiera-Garcia, Phys. Rev. D **96**(10), 104028 (2017). https://doi.org/10.1103/PhysRevD.96.104028

17. V.P. Frolov, G.A. Vilkovisky, Phys. Lett. B **106**, 307 (1981). https://doi.org/10.1016/0370-2693(81)90542-6

18. M. Ambrus, P. Hájíček, Phys. Rev. D **72**(6), 064025 (2005). https://doi.org/10.1103/PhysRevD.72.064025

19. C. Barceló, R. Carballo-Rubio, L.J. Garay, G. Jannes, Class. Quantum Gravity **32**(3), 035012 (2015). https://doi.org/10.1088/0264-9381/32/3/035012

20. C. Barceló, S. Liberati, S. Sonego, M. Visser, Phys. Rev. D **77**(4), 044032 (2008). https://doi.org/10.1103/PhysRevD.77.044032

21. S.D. Mathur, Class. Quantum Gravity **26**(22), 224001 (2009). https://doi.org/10.1088/0264-9381/26/22/224001

22. S.D. Mathur, D. Turton, J. High Energy Phys. **01**, 34 (2014). https://doi.org/10.1007/JHEP01(2014)034

23. B. Guo, S. Hampton, S.D. Mathur, J. High Energy Phys. **07**, 162 (2018). https://doi.org/10.1007/JHEP07(2018)162

24. R. Carballo-Rubio, F. Di Filippo, S. Liberati, M. Visser, Phys. Rev. D **98**(12), 124009 (2018). https://doi.org/10.1103/PhysRevD.98.124009

25. A. Simpson, M. Visser, J. Cosmol. Astropart. Phys. **2019**(2), 042 (2019). https://doi.org/10.1088/1475-7516/2019/02/042

26. H.G. Ellis, J. Math. Phys. **14**(1), 104 (1973). https://doi.org/10.1063/1.1666161

27. A. Simpson, P. Martín-Moruno, M. Visser, Class. Quantum Gravity **36**(14), 145007 (2019). https://doi.org/10.1088/1361-6382/ab28a5

28. F.S.N. Lobo, A. Simpson, M. Visser, Phys. Rev. D **101**(12), 124035 (2020). https://doi.org/10.1103/PhysRevD.101.124035

29. F.S.N. Lobo, M.E. Rodrigues, M.V. de S. Silva, A. Simpson, M. Visser, Phys. Rev. D **103**(8), 084052 (2021). https://doi.org/10.1103/PhysRevD.103.084052

30. M.S. Churilova, Z. Stuchlík, Class. Quantum Gravity **37**(7), 075014 (2020). https://doi.org/10.1088/1361-6382/ab7717

31. H.C.D.L. Junior, C.L. Benone, L.C.B. Crispino, Phys. Rev. D **101**(12), 124009 (2020). https://doi.org/10.1103/PhysRevD.101.124009

32. T.Y. Zhou, Y. Xie, Eur. Phys. J. C **80**(11), 1070 (2020). https://doi.org/10.1140/epjc/s10052-020-08661-w

33. P. Bambhaniya, K. Saurabh, Jusufi, P.S. Joshi, Phys. Rev. D **105**(2), 023021 (2022). https://doi.org/10.1103/PhysRevD.105.023021

34. J.R. Nascimento, A.Y. Petrov, P.J. Porfírio, A.R. Soares, Phys. Rev. D **102**(4), 044021 (2020)

35. N. Tsukamoto, Phys. Rev. D **103**(2), 024033 (2021). https://doi.org/10.1103/PhysRevD.103.024033

36. X.T. Cheng, Y. Xie, Phys. Rev. D **103**(6), 064040 (2021). https://doi.org/10.1103/PhysRevD.103.064040

37. M. Guerrero, G.J. Olmo, D. Rubiera-Garcia, D. Sáez-Chillón Gómez, J. Cosmol. Astropart. Phys. **2021**(8), 036 (2021). https://doi.org/10.1088/1475-7516/2021/08/036

38. E. Franzin, S. Liberati, J. Mazza, A. Simpson, M. Visser, J. Cosmol. Astropart. Phys. **2021**(7), 036 (2021). https://doi.org/10.1088/1475-7516/2021/07/036

39. S. Ray, A.L. Espíndola, M. Malheiro, J.P. Lemos, V.T. Zanchin, Phys. Rev. D **68**(8), 084004 (2003). https://doi.org/10.1103/PhysRevD.68.084004

40. R.M. Wald, Phys. Rev. D **10**, 1680 (1974). https://doi.org/10.1103/PhysRevD.10.1680

41. M. Zajaček, A. Tursunov, A. Eckart, S. Britzen, Mon. Not. R. Astron. Soc. **480**, 4408 (2018). https://doi.org/10.1093/mnras/sty2182

42. Y. Guo, Y.G. Miao (2021). arXiv e-prints. arXiv:2112.01747

43. Y. Guo, Y.G. Miao (2022). arXiv e-prints. arXiv:2201.02971

44. V. Perlick, Living Rev. Relativ. **7**, 9 (2004). https://doi.org/10.12942/lrr-2004-9

45. P. Schneider, J. Ehlers, E.E. Falco, *Gravitational Lenses* (Springer, Berlin, 1992). https://doi.org/10.1007/978-3-662-03758-4

46. A.O. Petters, H. Levine, J. Wambsganss, *Singularity Theory and Gravitational Lensing* (Birkhäuser, Boston, 2001). https://doi.org/10.1007/978-1-4612-0145-8

47. P. Schneider, C.S. Kochanek, J. Wambsganss, in *Saas-Fee Advanced Course 33: Gravitational Lensing: Strong, Weak and Micro*, ed. by G. Meylan, P. Jetzer, P. North (Springer, Berlin, 2006). https://doi.org/10.1007/978-3-540-30310-7

48. K.C. Sahu, J. Anderson, S. Casertano, H.E. Bond, P. Bergeron, E.P. Nelan, L. Pueyo, T.M. Brown, A. Bellini, Z.G. Levay, J. Sokol, M. Dominik, A. Calamida, N. Kains, M. Livio, Science **356**, 1046 (2017). https://doi.org/10.1126/science.aal2879

49. C.R. Keeton, A.O. Petters, Phys. Rev. D **72**(10), 104006 (2005). https://doi.org/10.1103/PhysRevD.72.104006

50. C.R. Keeton, A.O. Petters, Phys. Rev. D **73**(4), 044024 (2006). https://doi.org/10.1103/PhysRevD.73.044024

51. C.R. Keeton, A.O. Petters, Phys. Rev. D **73**(10), 104032 (2006). https://doi.org/10.1103/PhysRevD.73.104032

52. W.G. Cao, Y. Xie, Eur. Phys. J. C **78**, 191 (2018). https://doi.org/10.1140/epjc/s10052-018-5684-5

53. C. Darwin, Proc. R. Soc. A **249**, 180 (1959). https://doi.org/10.1098/rspa.1959.0015

54. K.S. Virbhadra, D. Narasimha, S.M. Chitre, Astron. Astrophys. **337**, 1 (1998)

55. K.S. Virbhadra, G.F.R. Ellis, Phys. Rev. D **62**(8), 084003 (2000)

56. V. Bozza, Phys. Rev. D **66**(10), 103001 (2002). https://doi.org/10.1103/PhysRevD.66.103001

57. E.F. Eiroa, G.E. Romero, D.F. Torres, Phys. Rev. D **66**(2), 024010 (2002). https://doi.org/10.1103/PhysRevD.66.024010

58. V. Bozza, Phys. Rev. D **67**(10), 103006 (2003). https://doi.org/10.1103/PhysRevD.67.103006

59. S.E. Vázquez, E.P. Esteban, Nuovo Cimento B Ser. **119**, 489 (2004). https://doi.org/10.1393/ncb/i2004-10121-y
60. N. Tsukamoto, Phys. Rev. D **95**(6), 064035 (2017). https://doi.org/10.1103/PhysRevD.95.064035
61. T. Hsieh, D.S. Lee, C.Y. Lin, Phys. Rev. D **103**(10), 104063 (2021). https://doi.org/10.1103/PhysRevD.103.104063
62. X. Lu, F.W. Yang, Y. Xie, Eur. Phys. J. C **76**, 357 (2016). https://doi.org/10.1140/epjc/s10052-016-4218-2
63. S.S. Zhao, Y. Xie, Eur. Phys. J. C **77**, 272 (2017). https://doi.org/10.1140/epjc/s10052-017-4850-5
64. S.S. Zhao, Y. Xie, Phys. Lett. B **774**, 357 (2017). https://doi.org/10.1016/j.physletb.2017.09.090
65. S. Chakraborty, S. SenGupta, J. Cosmol. Astropart. Phys. **7**, 045 (2017). https://doi.org/10.1088/1475-7516/2017/07/045
66. J.G. Cramer, R.L. Forward, M.S. Morris, M. Visser, G. Benford, G.A. Landis, Phys. Rev. D **51**(6), 3117 (1995). https://doi.org/10.1103/PhysRevD.51.3117
67. K.K. Nandi, Y.Z. Zhang, A.V. Zakharov, Phys. Rev. D **74**(2), 024020 (2006). https://doi.org/10.1103/PhysRevD.74.024020
68. C. Bambi, Phys. Rev. D **87**(10), 107501 (2013). https://doi.org/10.1103/PhysRevD.87.107501
69. K.K. Nandi, R.N. Izmailov, E.R. Zhdanov, A. Bhattacharya, J. Cosmol. Astropart. Phys. **2018**(7), 027 (2018). https://doi.org/10.1088/1475-7516/2018/07/027
70. K. Jusufi, N. Sarkar, F. Rahaman, A. Banerjee, S. Hansraj, Eur. Phys. J. C **78**(4), 349 (2018). https://doi.org/10.1140/epjc/s10052-018-5823-z
71. K. Jusufi, A. Övgün, Phys. Rev. D **97**(2), 024042 (2018). https://doi.org/10.1103/PhysRevD.97.024042
72. R. Shaikh, Phys. Rev. D **98**(2), 024044 (2018). https://doi.org/10.1103/PhysRevD.98.024044
73. R. Shaikh, P. Banerjee, S. Paul, T. Sarkar, Phys. Lett. B **789**, 270 (2019). https://doi.org/10.1016/j.physletb.2018.12.030
74. R. Shaikh, P. Banerjee, S. Paul, T. Sarkar, J. Cosmol. Astropart. Phys. **2019**(7), 028 (2019). https://doi.org/10.1088/1475-7516/2019/07/028
75. M. Amir, K. Jusufi, A. Banerjee, S. Hansraj, Class. Quantum Gravity **36**(21), 215007 (2019). https://doi.org/10.1088/1361-6382/ab42be
76. S. Sahu, M. Patil, D. Narasimha, P.S. Joshi, Phys. Rev. D **86**(6), 063010 (2012). https://doi.org/10.1103/PhysRevD.86.063010
77. R. Shaikh, P. Kocherlakota, R. Narayan, P.S. Joshi, Mon. Not. R. Astron. Soc. **482**(1), 52 (2019). https://doi.org/10.1093/mnras/sty2624
78. T. Kubo, N. Sakai, Phys. Rev. D **93**(8), 084051 (2016). https://doi.org/10.1103/PhysRevD.93.084051
79. P.V.P. Cunha, J.A. Font, C. Herdeiro, E. Radu, N. Sanchis-Gual, M. Zilhão, Phys. Rev. D **96**(10), 104040 (2017). https://doi.org/10.1103/PhysRevD.96.104040
80. M. Patil, P. Mishra, D. Narasimha, Phys. Rev. D **95**(2), 024026 (2017). https://doi.org/10.1103/PhysRevD.95.024026
81. R. Shaikh, P. Banerjee, S. Paul, T. Sarkar, Phys. Rev. D **99**(10), 104040 (2019). https://doi.org/10.1103/PhysRevD.99.104040
82. X.Y. Zhu, Y. Xie, Eur. Phys. J. C **80**(5), 444 (2020). https://doi.org/10.1140/epjc/s10052-020-8021-8
83. Y.X. Gao, Y. Xie, Eur. Phys. J. C **82**(2), 162 (2022). https://doi.org/10.1140/epjc/s10052-022-10128-z
84. Z. Horváth, L.Á. Gergely, Z. Keresztes, T. Harko, F.S.N. Lobo, Phys. Rev. D **84**(8), 083006 (2011). https://doi.org/10.1103/PhysRevD.84.083006
85. E.F. Eiroa, C.M. Sendra, Phys. Rev. D **86**(8), 083009 (2012). https://doi.org/10.1103/PhysRevD.86.083009
86. R.N. Izmailov, R.K. Karimov, E.R. Zhdanov, K.K. Nandi, Mon. Not. R. Astron. Soc. **483**(3), 3754 (2019). https://doi.org/10.1093/mnras/sty3350
87. F.Y. Liu, Y.F. Mai, W.Y. Wu, Y. Xie, Phys. Lett. B **795**, 475 (2019). https://doi.org/10.1016/j.physletb.2019.06.052
88. X. Lu, Y. Xie, Eur. Phys. J. C **79**(12), 1016 (2019). https://doi.org/10.1140/epjc/s10052-019-7537-2
89. X. Lu, Y. Xie, Eur. Phys. J. C **80**(7), 625 (2020). https://doi.org/10.1140/epjc/s10052-020-8205-2
90. Y.X. Gao, Y. Xie, Phys. Rev. D **103**, 043008 (2021). https://doi.org/10.1103/PhysRevD.103.043008
91. X. Lu, Y. Xie, Eur. Phys. J. C **81**(7), 627 (2021). https://doi.org/10.1140/epjc/s10052-021-09440-x
92. G. Nordström, Koninklijke Nederlandse Akademie van Wetenschappen **20**, 1238 (1918)
93. H. Reissner, Annalen der Physik **355**, 106 (1916). https://doi.org/10.1002/andp.19163550905
94. N. Dadhich, R. Maartens, P. Papadopoulos, V. Rezania, Phys. Lett. B **487**, 1 (2000). https://doi.org/10.1016/S0370-2693(00)00798-X
95. A. Cisterna, C. Erices, Phys. Rev. D **89**(8), 084038 (2014). https://doi.org/10.1103/PhysRevD.89.084038
96. E. Babichev, C. Charmousis, M. Hassaine, J. Cosmol. Astropart. Phys. **05**, 031 (2015). https://doi.org/10.1088/1475-7516/2015/05/031
97. A.F. Zakharov, F. de Paolis, G. Ingrosso, A.A. Nucita, Astron. Astrophys. **442**, 795 (2005). https://doi.org/10.1051/0004-6361:20053432
98. X. Pang, J. Jia, Class. Quantum Gravity **36**(6), 065012 (2019). https://doi.org/10.1088/1361-6382/ab0512
99. A.Y. Bin-Nun, Phys. Rev. D **81**(12), 123011 (2010). https://doi.org/10.1103/PhysRevD.81.123011
100. A.Y. Bin-Nun, Phys. Rev. D **82**(6), 064009 (2010). https://doi.org/10.1103/PhysRevD.82.064009
101. Z. Horváth, L.Á. Gergely, Astron. Nachr. **334**, 1047 (2013). https://doi.org/10.1002/asna.201211992
102. R. Whisker, Phys. Rev. D **71**(6), 064004 (2005). https://doi.org/10.1103/PhysRevD.71.064004
103. A.F. Zakharov, Phys. Rev. D **90**(6), 062007 (2014). https://doi.org/10.1103/PhysRevD.90.062007
104. C.Y. Wang, Y.F. Shen, Y. Xie, J. Cosmol. Astropart. Phys. **04**, 022 (2019). https://doi.org/10.1088/1475-7516/2019/04/022
105. S.S. Zhao, Y. Xie, J. Cosmol. Astropart. Phys. **07**, 007 (2016). https://doi.org/10.1088/1475-7516/2016/07/007
106. GRAVITY Collaboration, Astron. Astrophys. **602**, A94 (2017). https://doi.org/10.1051/0004-6361/201730838
107. Event Horizon Telescope Collaboration, Phys. Rev. Lett. **125**, 141104 (2020). https://doi.org/10.1103/PhysRevLett.125.141104
108. S. Weinberg, *Gravitation and Cosmology: Principles and Applications of the General Theory of Relativity* (Wiley, New York, 1972)
109. S. Refsdal, Mon. Not. R. Astron. Soc. **128**, 295 (1964). https://doi.org/10.1093/mnras/128.4.295
110. S. Gillessen, P.M. Plewa, F. Eisenhauer, R. Sari et al., Astrophys. J. **837**, 30 (2017). https://doi.org/10.3847/1538-4357/aa5c41
111. C.X. Huang, J. Burt, A. Vanderburg, M.N. Günther, A. Shporer, J.A. Dittmann, J.N. Winn, R. Wittenmyer, L. Sha, S.R. Kane, G.R. Ricker, R.K. Vanderspek, D.W. Latham, S. Seager, J.M. Jenkins, D.A. Caldwell, K.A. Collins, N. Guerrero, J.C. Smith, S.N. Quinn, S. Udry, F. Pepe, F. Bouchy, D. Ségransan, C. Lovis, D. Ehrenreich, M. Marmier, M. Mayor, B. Wohler, K. Haworth, E.H. Morgan, M. Fausnaugh, D.R. Ciardi, J. Christiansen, D. Charbonneau, D. Dragomir, D. Deming, A. Glidden, A.M. Levine, P.R. McCullough, L. Yu, N. Narita, T. Nguyen, T. Morton, J. Pepper, A. Pál, J.E. Rodriguez, K.G. Stassun, G. Torres, A. Sozzetti, J.P. Doty, J. Christensen-Dalsgaard, G. Laughlin, M. Clampin, J.L. Bean, L.A. Buchhave, G.Á. Bakos, B. Sato, S. Ida, L. Kaltenegger, E. Palle, D. Sasselov, R.P. Butler, J. Lissauer, J. Ge, S.A.

Rinehart, Astrophys. J. Lett. **868**, L39 (2018). https://doi.org/10.3847/2041-8213/aaef91

112. C.M. Claudel, K.S. Virbhadra, G.F.R. Ellis, J. Math. Phys. **42**, 818 (2001). https://doi.org/10.1063/1.1308507

113. D. Psaltis, F. Özel, C.K. Chan, D.P. Marrone, Astrophys. J. **814**, 115 (2015). https://doi.org/10.1088/0004-637X/814/2/115

114. V. Bozza, S. Capozziello, G. Iovane, G. Scarpetta, Gen. Relativ. Gravit. **33**, 1535 (2001). https://doi.org/10.1023/A:1012292927358

115. V. Bozza, L. Mancini, Gen. Relativ. Gravit. **36**, 435 (2004). https://doi.org/10.1023/B:GERG.0000010486.58026.4f

116. K.A. Bronnikov, R.K. Walia, Phys. Rev. D **105**(4), 044039 (2022). https://doi.org/10.1103/PhysRevD.105.044039

117. J. Ibanez, Astron. Astrophys. **124**, 175 (1983)

118. I. Bray, Phys. Rev. D **34**, 367 (1986). https://doi.org/10.1103/PhysRevD.34.367

119. S.A. Klioner, Sov. Astron. **35**, 523 (1991)

120. J.F. Glicenstein, Astron. Astrophys. **343**, 1025 (1999)

121. M. Sereno, F. De Luca, Phys. Rev. D **74**(12), 123009 (2006). https://doi.org/10.1103/PhysRevD.74.123009

122. M.C. Werner, A.O. Petters, Phys. Rev. D **76**(6), 064024 (2007). https://doi.org/10.1103/PhysRevD.76.064024

123. M. Sereno, F. De Luca, Phys. Rev. D **78**(2), 023008 (2008). https://doi.org/10.1103/PhysRevD.78.023008

124. A.B. Aazami, C.R. Keeton, A.O. Petters, J. Math. Phys. **52**(9), 092502 (2011). https://doi.org/10.1063/1.3642614

125. A.B. Aazami, C.R. Keeton, A.O. Petters, J. Math. Phys. **52**(10), 102501 (2011). https://doi.org/10.1063/1.3642616

126. G. He, W. Lin, Int. J. Mod. Phys. D **23**, 1450031 (2014). https://doi.org/10.1142/S021827181450031X

127. G. He, C. Jiang, W. Lin, Int. J. Mod. Phys. D **23**, 1450079 (2014). https://doi.org/10.1142/S0218271814500795

128. X.M. Deng, Int. J. Mod. Phys. D **24**, 1550056 (2015). https://doi.org/10.1142/S021827181550056X

129. G.S. He, W.B. Lin, Res. Astron. Astrophys. **15**, 646 (2015). https://doi.org/10.1088/1674-4527/15/5/003

130. X.M. Deng, Int. J. Mod. Phys. D **25**, 1650082 (2016). https://doi.org/10.1142/S0218271816500826

131. G. He, W. Lin, Phys. Rev. D **93**(2), 023005 (2016). https://doi.org/10.1103/PhysRevD.93.023005

132. G. He, W. Lin, Phys. Rev. D **94**(6), 063011 (2016). https://doi.org/10.1103/PhysRevD.94.063011

133. G. He, W. Lin, Class. Quantum Gravity **33**(9), 095007 (2016). https://doi.org/10.1088/0264-9381/33/9/095007

134. G. He, W. Lin, Class. Quantum Gravity **34**(10), 105006 (2017). https://doi.org/10.1088/1361-6382/aa691d

135. G. He, C. Pan, W. Lin, Eur. Phys. J. C **79**(8), 705 (2019). https://doi.org/10.1140/epjc/s10052-019-7217-2

136. S.E. Gralla, Phys. Rev. D **103**, 024023 (2021). https://doi.org/10.1103/PhysRevD.103.024023

137. M.D. Johnson, A. Lupsasca, A. Strominger, G.N. Wong, S. Hadar, D. Kapec, R. Narayan, A. Chael, C.F. Gammie, P. Galison, D.C.M. Palumbo, S.S. Doeleman, L. Blackburn, M. Wielgus, D.W. Pesce, J.R. Farah, J.M. Moran, Sci. Adv. **6**(12), eaaz1310 (2020). https://doi.org/10.1126/sciadv.aaz1310

138. S.E. Gralla, A. Lupsasca, Phys. Rev. D **102**, 124003 (2020). https://doi.org/10.1103/PhysRevD.102.124003

139. S.E. Gralla, A. Lupsasca, D.P. Marrone, Phys. Rev. D **102**, 124004 (2020). https://doi.org/10.1103/PhysRevD.102.124004

140. S.E. Gralla, D.E. Holz, R.M. Wald, Phys. Rev. D **100**(2), 024018 (2019). https://doi.org/10.1103/PhysRevD.100.024018

141. M. De Laurentis, R. De Rosa, F. Garufi, L. Milano, Mon. Not. R. Astron. Soc. **424**, 2371 (2012). https://doi.org/10.1111/j.1365-2966.2012.21410.x

142. X.M. Deng, Europhys. Lett. **120**(6), 60004 (2017). https://doi.org/10.1209/0295-5075/120/60004

143. X.M. Deng, Eur. Phys. J. Plus **132**, 85 (2017). https://doi.org/10.1140/epjp/i2017-11376-1

144. I. De Martino, R. Lazkoz, M. De Laurentis, Phys. Rev. D **97**(10), 104067 (2018). https://doi.org/10.1103/PhysRevD.97.104067

145. M. De Laurentis, I. De Martino, R. Lazkoz, Phys. Rev. D **97**(10), 104068 (2018). https://doi.org/10.1103/PhysRevD.97.104068

146. M. De Laurentis, I. De Martino, R. Lazkoz, Eur. Phys. J. C **78**(11), 916 (2018). https://doi.org/10.1140/epjc/s10052-018-6401-0

147. W. Li, B. Yang, C. Ma, X. Zhou, Z. Feng, G. He, Mod. Phys. Lett. A **36**(22), 2150164 (2021). https://doi.org/10.1142/S0217732321501649

148. J. Levin, G. Perez-Giz, Phys. Rev. D **77**(10), 103005 (2008). https://doi.org/10.1103/PhysRevD.77.103005

149. J. Levin, R. Grossman, Phys. Rev. D **79**(4), 043016 (2009). https://doi.org/10.1103/PhysRevD.79.043016

150. J. Levin, G. Perez-Giz, Phys. Rev. D **79**(12), 124013 (2009). https://doi.org/10.1103/PhysRevD.79.124013

151. J. Levin, Class. Quantum Gravity **26**(23), 235010 (2009). https://doi.org/10.1088/0264-9381/26/23/235010

152. V. Misra, J. Levin, Phys. Rev. D **82**(8), 083001 (2010). https://doi.org/10.1103/PhysRevD.82.083001

153. B. Gao, X.M. Deng, Ann. Phys. **418**, 168194 (2020). https://doi.org/10.1016/j.aop.2020.168194

154. X.M. Deng, Eur. Phys. J. C **80**(6), 489 (2020). https://doi.org/10.1140/epjc/s10052-020-8067-7

155. X.M. Deng, Phys. Dark Universe **30**, 100629 (2020). https://doi.org/10.1016/j.dark.2020.100629

156. H.Y. Lin, X.M. Deng, Phys. Dark Universe **31**, 100745 (2021). https://doi.org/10.1016/j.dark.2020.100745

157. Bo. Gao, Xue-Mei. Deng, Eur. Phys. J. C **81**(11), 983 (2021). https://doi.org/10.1140/epjc/s10052-021-09782-6

158. Bo. Gao, Xue-Mei. Deng, Mod. Phys. Lett. A **36**(33), 2150237 (2021). https://doi.org/10.1142/S0217732321502370

159. H.Y. Lin, X.M. Deng, Eur. Phys. J. Plus **137**(2), 176 (2022). https://doi.org/10.1140/epjp/s13360-022-02391-6

160. J. Zhang, Y. Xie, Astrophys. Space Sci. **367**(2), 17 (2022). https://doi.org/10.1007/s10509-022-04046-5